Norwegian Meteorological Institute
met.no
met.no report

no. 20/2005
Climate

Storm Frequencies over Fennoscandia - Relevance for Bark beetle outbreak

RegClim results

Rasmus E. Benestad

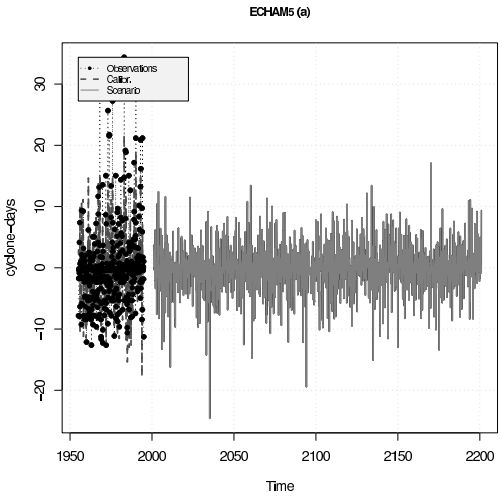

Norwegian Meteorological Institute
met.no

report

Title	Date
Future Storm Frequencies over Fennoscandia - Relevance for Bark beetle outbreak	20th December 2005
Section Climate	**Report no.** 20/2005
Author Benestad	**Classification** ● Free ○ Restricted
	ISSN 1503-8025
	e-ISSN 1503-8025
Client(s) Bjørn Økland, Skogforsk (project 155893/720 NORKLIMA, NFR)	**Client's reference**

Abstract

Mid-latitude storms are analysed using a Calculus-based Cyclone Identification (CCI) method, and tentative simple linear trend models are derived from both historical analysis (observations) as well as from climate model data. Linear trend models for the most extreme and infrequent cyclones are derived using an extrapolation from weaker and more frequent to intense and rare storms, assuming a slow manifold which converges to zero at low central pressures. Global and regional climate models' ability to represent cyclones are examined. The CCI analysis was applied to different data sets and different models.

A tentative conclusion is arrived at, however, it is important to stress that the estimates are associated with high degree of uncertainty and should at present stage be regarded as a sketchy best guess: (i) Historical analyses give indications of an increase in the number of cyclones over Fennoscandia over the recent 40–50 years and (ii) The analysis of climate model results may indicate that future frequency of cyclones may be at a higher level than at present.

Keywords

Mid-latitude storms, CCI, hidtorical analysis, moel simulations, climate change.

Disciplinary signature	Responsible signature
Eirik Førland	Cecilie Mauritzen

Postal address P.O Box 43 Blindern, N-0313 OSLO, Norway
Office Niels Henrik Abels vei 40
Telephone +47 2296 3000
Telefax +47 2296 3050
e-mail: met.inst@met.no **Internet:** met.no
Bank account 7694 05 00601
Swift code DNBANOKK

Contents

1 Introduction

Intense cyclones such as mid-latitude (also known as 'extra-tropical') storms may cause extensive damage. For forestry, wind felling caused by powerful storms occur episodic and can trigger subsequent outbreaks of bark beetle epidemics (*Økland & Bjørnstad*, in press, 2003; *Økland & Berryman*, 2004). It is therefore of great interest to be able to forecast frequencies and intensities of storms in the future.

The objective of this study is to explore climate change scenarios from global climate models (GCMs) and regional climate models (RCMs) in order answer the question whether it is likely that a future global warming will produce more or stronger storms over Fennoscandia. Also, it is important to assess the degree of realism to which climate models can represent mid-latitude storm systems.

Here the terms 'storm', 'low-pressure system' and 'cyclone' will be used, all of which referring to mid-latitude storms. Very intense cyclones have been known to cause extensive windfall damage to forests, and such extensive windfalls can trigger outbreak of bark beetle (*Økland & Bjørnstad*, in press, 2003; *Økland & Berryman*, 2004). A change in the frequency of such powerful storms will therefore be a part of assessments for the future based on scenarios from climate models.

Some climate models suggest that a global warming may be favourable for more intense mid-latitude storms (*Ulbrich & Christoph*, 1999). Model simulations performed by *Knippertz* et al. (2000) suggests that anthropogenic global warming may shift the storm track north- and eastward, as well as leading to an increase in the frequency of intense (defined as cyclones with central pressure below 970 hPa) and decrease in the number of weak storms. There are also a couple of physics-based considerations that can provide an indication of the main features: (i) As the surface and atmosphere warm up, more energy (heat) becomes available in the form of water vapour (more evaporation and the air manages to hold more moisture), but (ii) one factor which may act as a moderating influence, is that a global warming is expected to warm the polar regions faster than the lower latitudes, hence reducing the meridional (north-south) temperature differences (gradient). Mid-latitude storms tend to be associated with baroclinic instabilities, related to horizontal temperature gradients: the storms tend to form where there are sharp temperature gradients, where conditions for instabilities are favourable. There tend to be a sharp temperature drop poleward of the polar fronts, and it is no coincidence that this is the same region where the storm tracks are located.

The mid-latitude storms play an important role in the climate system, as they facilitate the poleward heat transport (*Trenberth & Stepaniak*, 2004; *Hartmann*, 1994; *Peixoto & Oort*, 1992). Hence, we would expect to see a relationship between the number of storms and the pole-equator temperature differences. A hand-wavy argument is that an enhanced high-latitude warming weakens the conditions favouring baroclinic instabilities, and hence fewer storms may form (other factors being constant). Another side of the picture may be that part of the reason why the poles warm more strongly than the lower latitudes (in addition to reduced sea-ice) is due to an increase in storm activity along the storm tracks. *Trenberth & Stepaniak* (2004) argued that there is a 'seamless' equator-to-pole energy flow that is responsible for higher temperatures in the polar region than a pure energy balance would imply. Cyclones are responsible for the eddy heat transport in the mid-latitudes, however the energy flow does not just depend on their frequency and intensity but also on their spatial structure.

Past observations suggests that changes in the storm statistics may be associated with a displacement of the storm tracks. This kind of change points to the importance of correct simulation of the storm tracks in the climate models. A shift in simulated storm track may give incorrect impression about the change in

storminess if the model does not give a correct description of the present-day storm track in the simulation for present conditions.

2 Methods

Here a mathematical method henceforth referred to as Calculus-based Cyclone Identification (CCI) is used to identify and keep track of the individual cyclones. The method involves a truncated Fourier series to approximate north–south and east–west sea level pressure (SLP) profiles, and ordinary multiple regression to estimate the values of the Fourier coefficients. The CCI method is described in *Benestad & Chen* (submitted), but a similar method was also employed in the analysis presented in *Benestad* (2005a,b); *Benestad & Hanssen-Bauer* (2003). The CCI-analysis was implemented using the package `cyclones` from CRAN (http://cran.r-project.org).

The data analysed here consisted of gridded SLP at 12-hour or 24-hour intervals. These time resolutions are to some degree crude for cyclone analysis, as the storm systems tend to move some distance within a half a day. Although a higher time resolution (eg 6-hour) would be preferable, this would entail greater demand for data storage, longer time for the analysis, and probably not yield a very different picture as the 12 and 24-hour data. Furthermore, much of the data from the GCMs is not available for the general scientific community on time resolutions higher than 24 hours. The 12-hour SLP was taken from the NMC (former National Meteorological Center, now National Center for Environmental Prediction, NCEP) analysis and 24-hour data from the re-analysis (*Simmons & Gibson*, 2000), henceforth referred to as 'ERA40', from the European Centre for Medium-range Weather Forecasts (ECMWF).

There are other methods for analysing cyclones involving the vorticity, however, the use of vorticity involves a number of choices such as baroclinic or barotropic vorticity, relative ($\zeta = \partial v/\partial x - \partial u/\partial y$), absolute ($\zeta + f$), or potential ($Q' = \zeta/H - f\eta/H^2$, where H is the scale height and η is the height displacement of the geopotential height surface), and the altitude level at which it is computed. Whereas the vorticity is a computed product from atmospheric models, it is not directly observed in the historical observations. Furthermore, the vorticity is not as commonly archived on open access data bases. For a geostropic flow ($u_g = -\frac{\partial p/\partial y}{f\rho}$, $v_g = \frac{\partial p/\partial x}{f\rho}$) and SLP data, then the relative vorticity is

$$\zeta = \frac{1}{f\rho}\left(\frac{\partial^2 p}{\partial x^2} + \frac{\partial^2 p}{\partial y^2}\right) = \frac{1}{f\rho}\nabla^2 p, \tag{1}$$

p being SLP. Thus, the use of vorticity as a variable to indicate cyclonic acticity would involve differentiation twice before obtaining a vortex field which can be analysed, and then subsequent differentiation is required to find local maxima and minima. Thus an imperfect approximation would be prone to a greater risk of introducing errors. The inclusion of the scale height H requires extra information normally not available for historical gridded analysis or archived model results. Thus, the a direct application of the CCI method on the SLP is likely the best method for analysing cyclones in this case.

When it is not possible to provide very accurate estimates for cyclone trends, it may be more useful to provide upper and lower limits to the range in which the trends must lie. Here, these limits are determined by the trends estimates for weaker and more frequent cyclones as well as the expectation that the number of very deep cyclones converge to zero as the intensity increases.

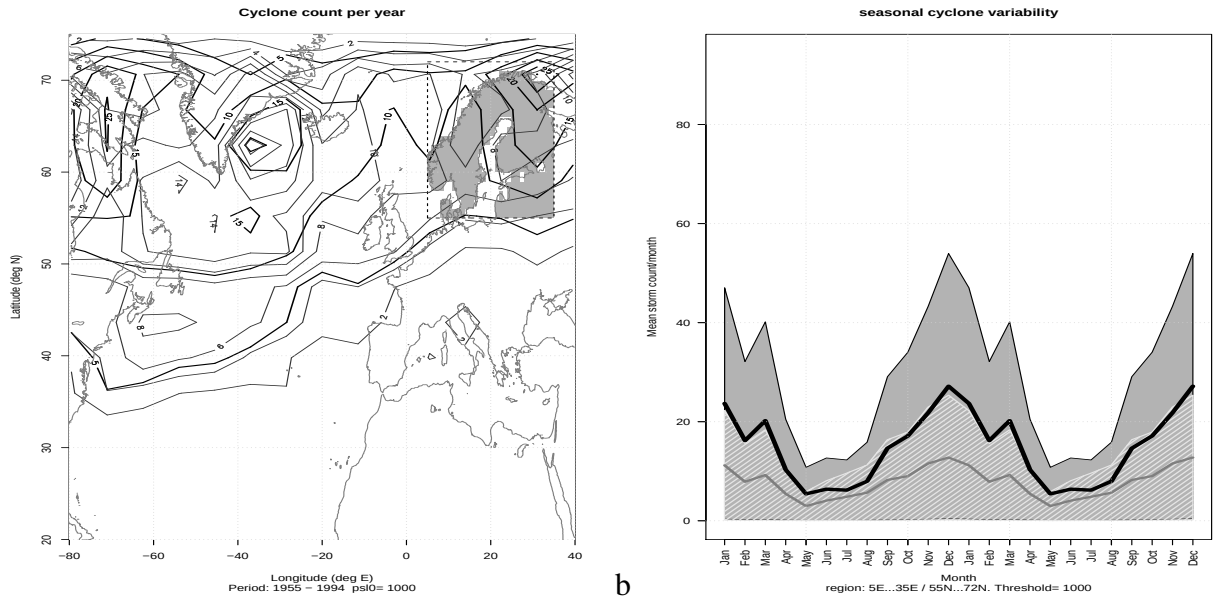

Figure 1: The geographical variation in storm frequency (a) and annual variation in storm frequency in the 5°E–35°E/55°N–72°N-region (grey shaded region) (b) from ERA40 (thin contours and grey thin curve) and NMC (thick contours and fat black curve). The shading shows the year-to-year standard deviation (grey for NMC, white hatched for ERA40).

Several different avenues have been explored in the analysis of cyclone trends in this report:

(i) By using the CCI-method for case studies of known windfalls.

(ii) By 'downscaling' cyclone counts based on monthly SLP fields.

(iii) By using CCI to explore geographical distribution and annual cycle of mid-latitude storm densities in the GCMs and RCMs.

(iv) CCI used to count the evolution of storm counts within a defined region to infer best linear trend models $N = \alpha + \beta t$ for a set of threshold values.

(v) Use the estimates for α and β for different central pressures thresholds to interpolate to more intense storms, assuming that both converge to zero for SLP less than 950hPa.

The GCM data were obtained from the Program for Climate Model Diagnoses and Intercomparison - PCMDI: https://esg.llnl.gov:8443/index.jsp. The RCM data were taken from the PRUDENCE home page: http://prudence.dmi.dk/

3 Results

3.1 'Observations': Storm statistics from re-analysis

Figure 1 shows cyclone statistics derived with `cylones`, based on gridded sea level pressure (SLP) from NMC and ERA40. Panel a shows the frequency density, exhibiting the well-known North-Atlantic storm

track region near Iceland and south of Greenland. It is interesting to note similar cyclone densities over the northwestern part of the North Atlantic, and contrast these to the different densities obtained from NMC and ERA40 over the Fennoscandic region (grey hatched). The NMC data yields an increase in the frequency over northeastern Fennoscandia that is not seen in the ERA40 CCI analysis, a feature that is likely to be false. These differences illustrate some of the uncertainties associated with the cyclone analysis. The annual variation in the number of storms deeper than 1000hPa over Fennoscandia (shaded region on panel a) is shown in panel b: the storm activity peaks in winter and is low in summer. There may be several reasons for the differences between the CCI results derived for Fennoscandia based on NMC and ERA40: (i) different spatial resolution in the re-analysis/analysis may affect the representation of cyclones, (ii) difference in data assimilation and atmospheric models involved, (iii) the effect of topography on the analysis (including simulation) and observed values of the pressure (reduced to sea level), (iv) different time periods, and (v) different underlying observational material.

These characteristics can be used to assess the degree of realism of the results derived from GCMs. It is important that the GCMs reproduce the storm track features in the correct location for making projections about future storm patterns given a climate change. Furthermore, a correct simulation of the seasonal variation is an important lackmus test of whether the GCMs are capable of simulating a realistic response to a (seasonally) environment.

3.1.1 Historical accounts on wind felling

A number of severe windfall events affecting Norwegian forestry are listed in Table 1. Intense cyclones causing widespread windfalls and forest damage will be referred to as 'severe storms' in this report. In order to assess whether the CCI statistics applied to the gridded SLP is an appropriate approach for making projections about severe storm frequencies, it is necessary to check whether the CCI method is able to pick out storms that were associated with historical windfalls. Factors other than wind can also cause windfalls (*Skog & Forskning*, 1995), however, strong wind is assumed to be the most decisive factor. Only large windfall episodes covering large areas appear to be significant for bark beetle populations that are synchronized at regional scale levels (*Økland & Bjørnstad*, 2003). It is important to estimate the intensities of the storms causing the damages as well as the distance between the storm centre and the damages. The most intense and potentially most damaging winds are not necessarily located at the storm centre, but tend to be where the pressure gradient is sharpest, and storms may therefore have a significant cross-section for potential damage. Figures 2–3 show the cases for the major and 'minor' storms associated with the windfalls in Table 1.

The location and trajectory of the central pressure in the historical storms of November 10 1969 (south-eastern Norway), October 16 1987 (south-eastern Norway) and January 1 1992 (northern Norway) which resulted in extensive windfall damages are shown in Figure 2. The corresponding central pressures were 977–980, 971–973, and 970–984 hPa respectively. The trajectory for the central location of the storm of October 16 1987, also known as 'Great Storm of 1987', did not cross the Norwegian mainland and corresponds with other analyses found on the Internet (*Benestad & Chen*, submitted). Hence, powerful storms may result in widespread windfall damage within a distance away from the storm centre. The storm of 1992 moved rapidly across the Greenland-Iceland and Norwegian Sea (GIN Sea), but the impression given by Figure 2c is exaggurated due to the longitudinal stretching of the longitudes in the map projection.

The wind energy (speed) is related to the radius and pressure gradients, and therefore not directly related

Year	Date	volume (m^3)	Region	Comments
Major events:				
1969	10.–11.Nov	2,400,000	Østlandet	Triggered bark beetle outbreak in the 1970s
1987	16. Oct	1,800,000	Østlandet	The only windfall associated with bark beetle population growth 1979–2000 (Økland & Berryman, 2004)
1992	1. Jan	1,800,000	Nordvestlandet	Extensive damages; a region where the spruce bark beetle is not commo
Minor events:				
1949	Okt	?	N. Hedmark	Femunden accounted for 50,000 m^3 damage (mostly mountain forest)
1957	?	?	Sør- og Østlandet	Extensive damages in Sør- & Østlandet reported. No effect on the bark beetle population
1975/1976	?	?	Østlandet	Moderate windfalls; most i Vestfold
1999	1-Dec	?	Østlandet, Østfold, Akershus Søndre Buskerud, Oppland, Hedmark.	No significant effect on the bark beetle population.
2000	17-Jan	?	Telemark, Vestfold, Buskerud	No significant effect on the bark beetle population.
2000	slutt okt	300,000	N.Trøndelag og søndre Nordland	Decline in the bark beetle population in i N. Trøndelag (2002), data for Nordland missing before 2002, but some increase subsequent to 2003
2001	16-Aug	140,000	Østlandet	Tornado sweeps produced local strips between Drammen and Koppang. No significant effect on the bark beetle population.
2001	15-Nov	330,000	Telemark, Buskerud, Oppland	No significant effect on the bark beetle population.
2003	6-Dec	318,000	Akershus, Hedmark, Østfold	Akershus 45,000m^3, Hedmark 223,000m^3, Østfold 50,000m^3; a small increase in bark beetle populations were recorded in 2005

Table 1: A list of severe windfalls in Norway (compiled by Bjørn Økland, Erik Christiansen and Skogbrand).

to the central pressure depth, but the central pressure shown here gives some indication about the storm severity. The case studies for the minor incidents listed in Table 1, shown in Figure 3, have central pressures below 990hPa. Hence, it is reasonable to define storms with central pressure deeper than 970hPa as severe storms with high destructive potential and storms deeper than 990hPa as more moderate, but still potentially damaging storms.

Figure 4 provides a number of intense storm cases in the vicinity of Oslo. It is clear that the number of intense storms is low (12) for the 1955–1994, averaging one storm every 3.25 year. This low number implies that a trend analysis for intense storms will be associated with a high degree of uncertainty.

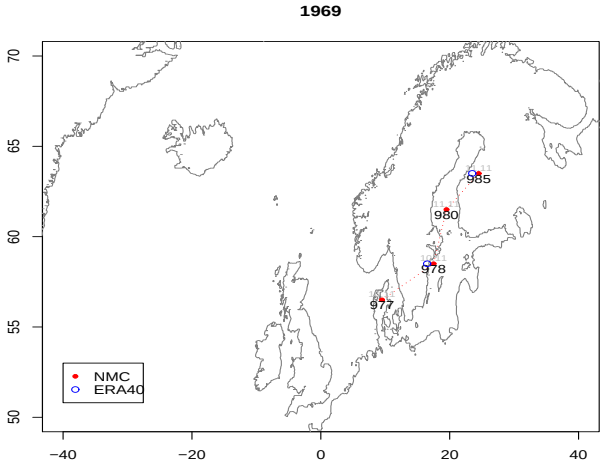

a

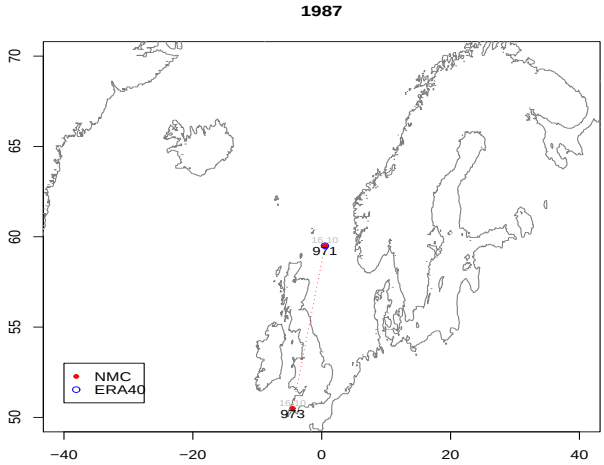

b

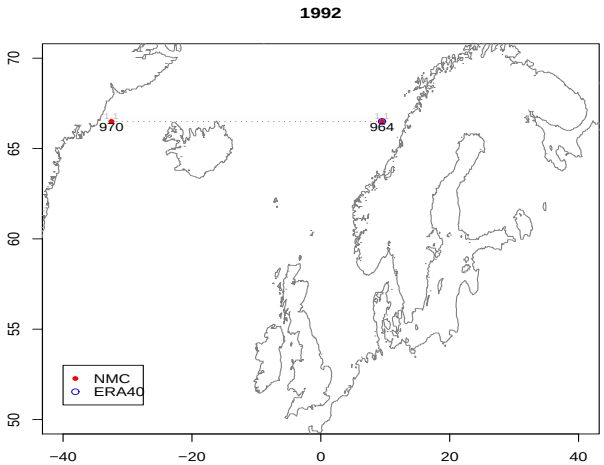

c

Figure 2: Storm locations for historical storms of November 10 1969 (a), October 16 1987 (b) and January 1 1992 (c) derived from CCI-analysis applied to NMC analysis (every 12 hour) and ERA-40 re-analysis (every 24 hour).

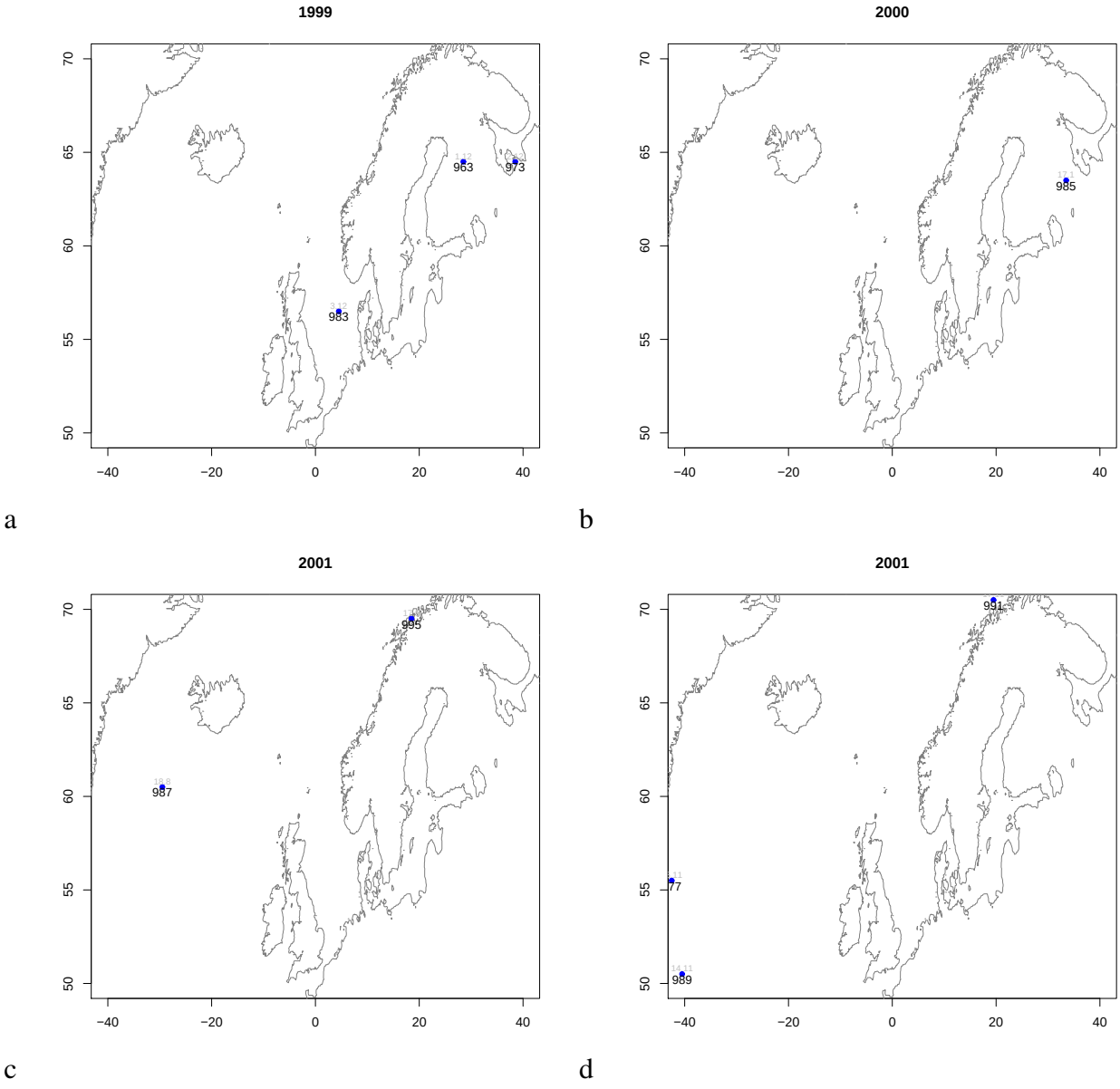

Figure 3: Maps showing the location of minor storms according to CCI applied to ERA40 SLP.

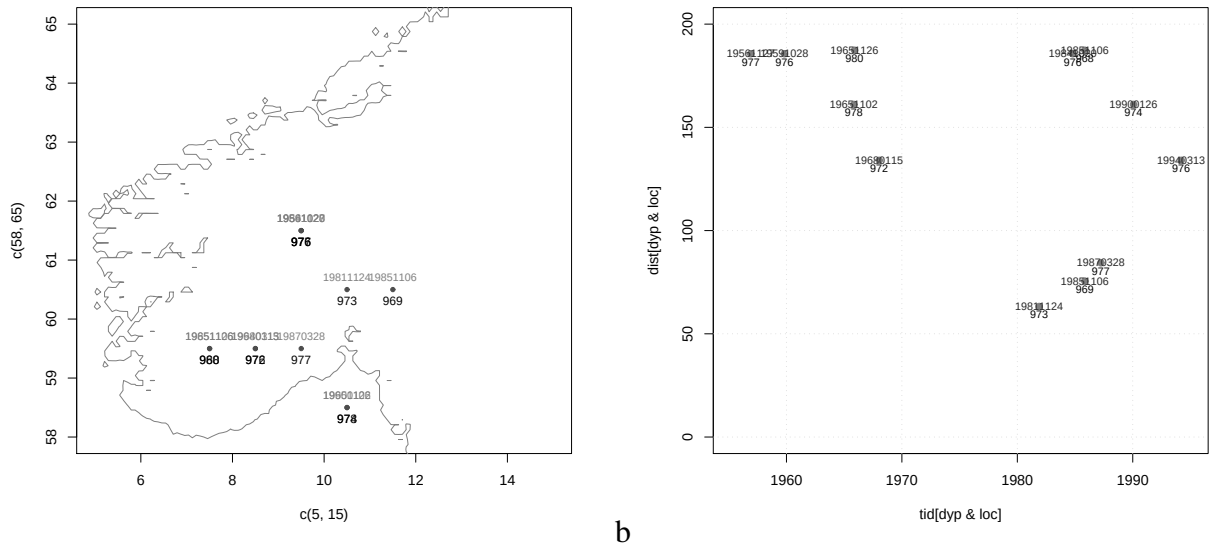

Figure 4: A summary of historical cyclones within a 200km radius of Oslo that had a central pressure deeper than 980hPa. (a) location of the cyclones and (b) distance from Oslo. The central pressure are listed in the figure. THe time interval for the analysis was 1955–1994.

3.2 Multi-model 'downscaling' based on monthly mean SLP

The multi-model 'downscaling' analysis involved the use of monthly SLP from GCMs and an application of a regression analysis to monthly cyclone counts from CCI (NMC) in order to provide a crude assessment of systematic changes in the storm tracks. The model is the same as being used in regular downscaling (*Benestad*, 2004), although statistically modelling of cyclones is not described in terms of 'downscaling' in traditional sense. This discussion will nevertheless stick to the term 'downscaling model' here, as the model has the same mathematical framework as those used to downscale local temperature.

If low-pressure systems become more frequent and/or more intense over a given region (here Fennoscandia), then such a change is expected to make an imprint in the regional monthly mean SLP as negative SLP anomalies. The downscaling model has been validated against observations (*Benestad & Chen*, submitted) and shown to reproduce a large portion of the monthly storm frequency. Negative SLP anomalies are translated to higher numbers of cyclones by the downscaling model.

Figure 5 shows 'downscaled' results for the CCI cyclone statistics based on the BCM, HadGEM1, HadCM3, ECHAM5, GFDL and NCAR-CCSM climate models following the IPCC SRES A2 or A1b emission scenarios. The time series in the left panels show both statistics based on past observations (NMC; black) as well as model reproduction of the results. The variance in the cyclone count derived from the BCM SLP is weaker than the observed variance (grey curve in Figure 5a) as a result of too weak SLP anomalies in the model. The HadGEM1, on the other hand, produced a storm statistics with greater variance (Figure 5c; grey), as opposed to the HadCM3 model (Figure 5e; grey) with too weak variations. The ECHAM5 models (Figure 5g,i & k; grey) also gave too low variance. A discrepancy in the variance can partly be explained in terms of the statistical model itself - that it cannot account for most of the variance, as manifested in low R^2-statistics (blue curve in right panels) - and partly as a result of the behaviour of the gridded SLP in the GCMs.

The strength of the regression (high R^2 statistics and a large fraction of variance accounted for) tends to be high for the winter- and low for the summer season (blue curve in right panels). Overall, the multi-model ensemble of GCMs do not indicate much trend as there is little common tendency, but one interesting common feature is that all these results suggest a positive trend in February and March. There is a substantial scatter in the results derived from one GCM (ECHAM5: Figure 5g–l), with one scenario producing a strong negative trend for January (probably a spurious spike: Figure 5i–j).

There is no overall trend in these analysed time series, as the models do not predict a systematic displacement of the air masses and the SLP does not provide a clear climate signal (*Benestad*, 2002). Thus, the downscaling of cyclones from monthly mean SLP may not be an appropriate approach if a change in the storm statistics does not significantly impact the mean state.

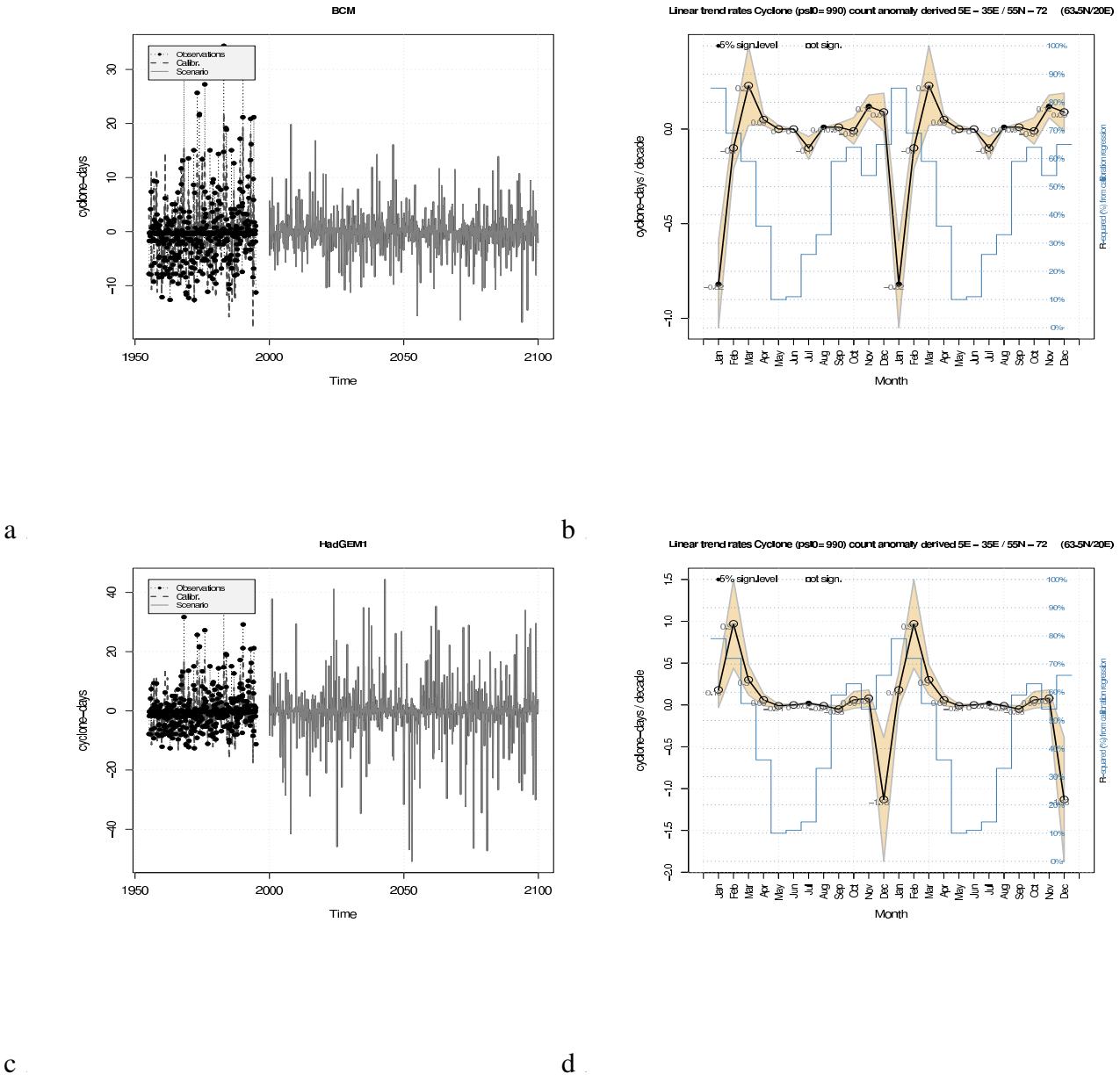

Figure 5: 'Downscaled' monthly storm count for the 5°E–35°E/55°N–72°N-region (grey shaded region). Left panels show the time series whereas the right panels indicate the rate of change in storm frequency and strength of the regression (R^2). The cyclone statistics represent systems with estimated central lower than 900hPa derived from the NMC gridded analysis. Two cycles are shown by repeating the calendar month twice. The results are for the SRES A1b scenario for all models except for BCM (which followed the A2-emission line). (a–b) BCM and (c–d) HadGEM1.

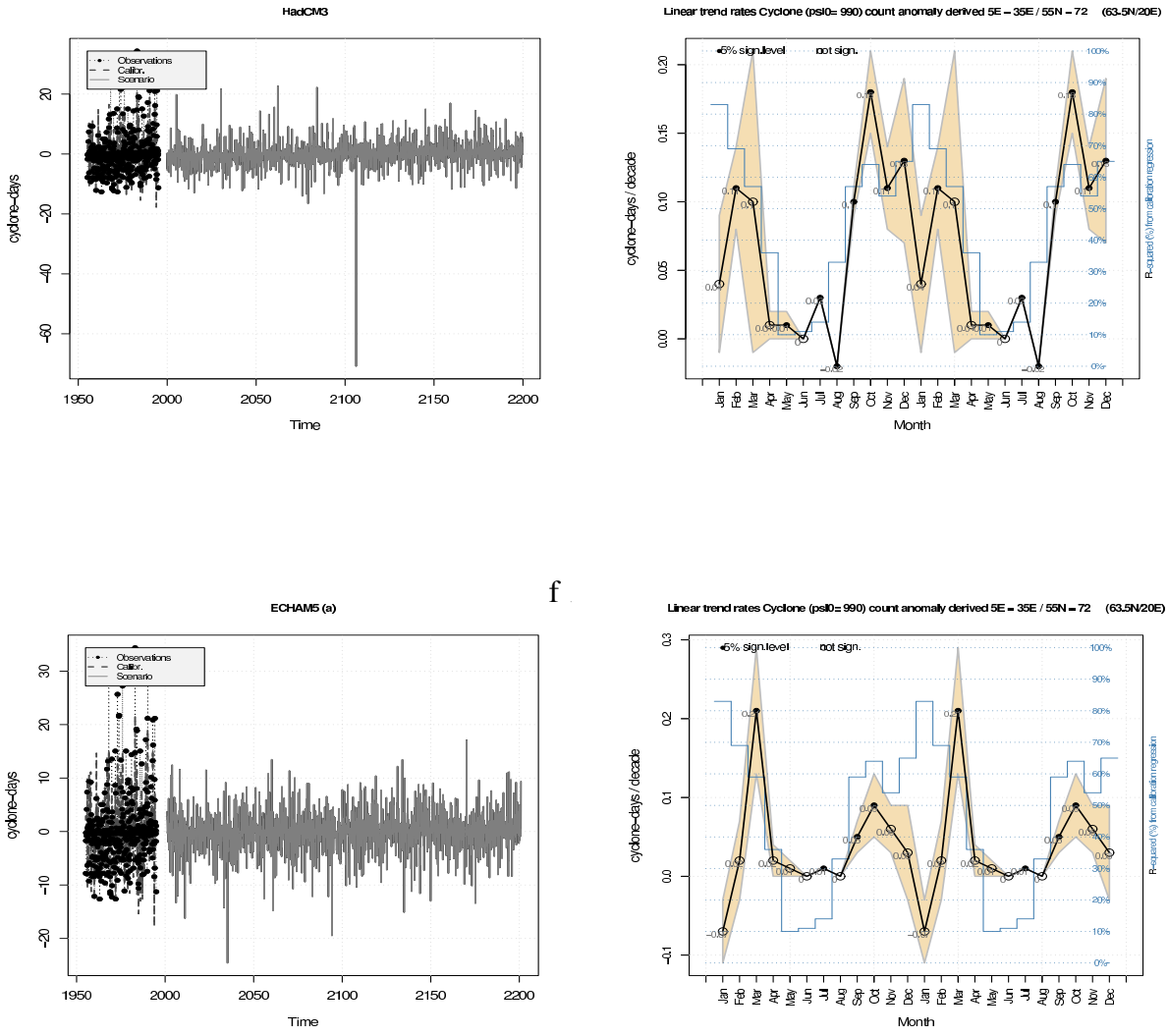

e f

g h

Figure 5: Figure continued. The results are for HadCM3 (upper) and ECHAM5 run 1 (lower).

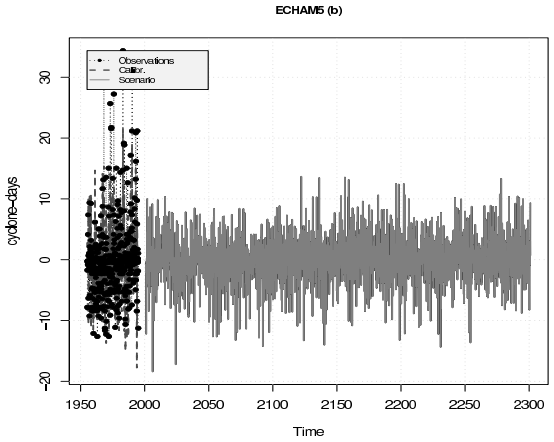

i

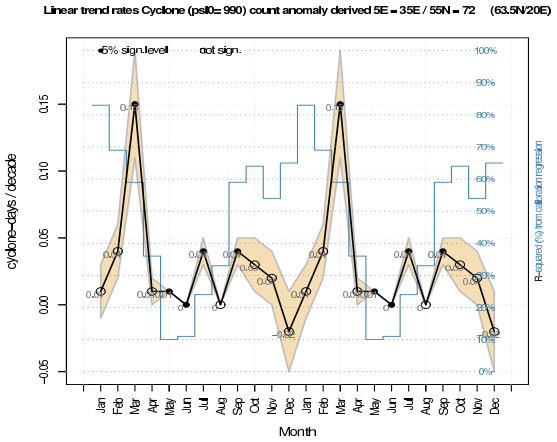

j

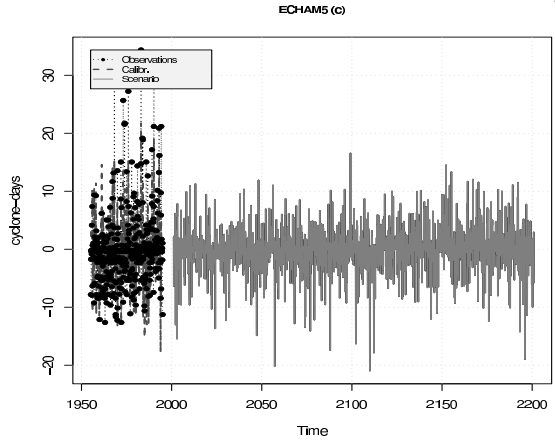

k

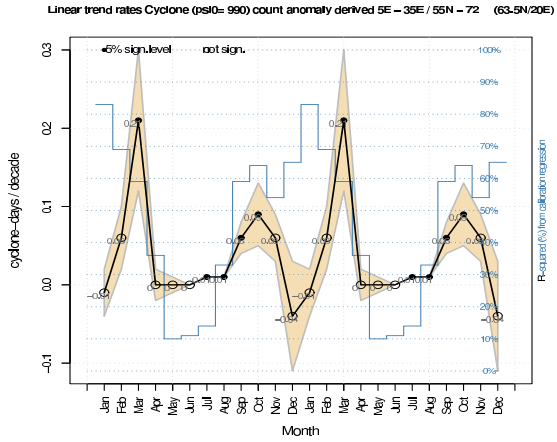

l

Figure 5: Figure continued. The results are for ECHAM5 run 2 (upper) and ECHAM5 run 3 (lower).

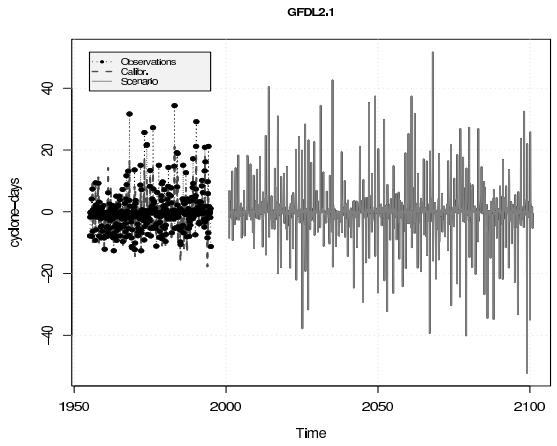

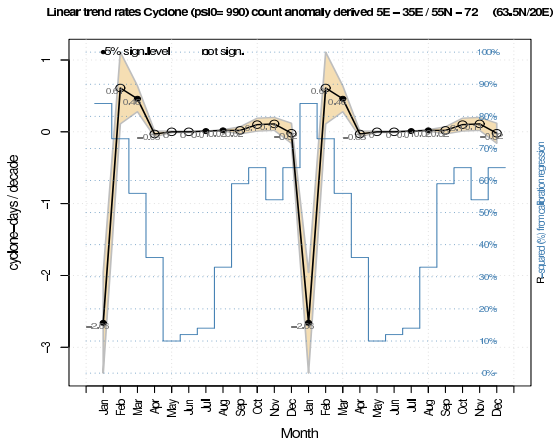

m

n

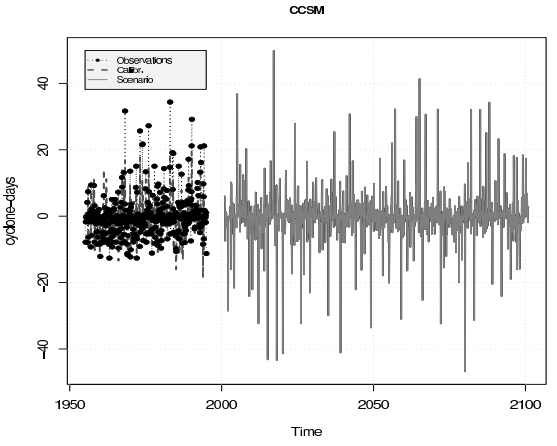

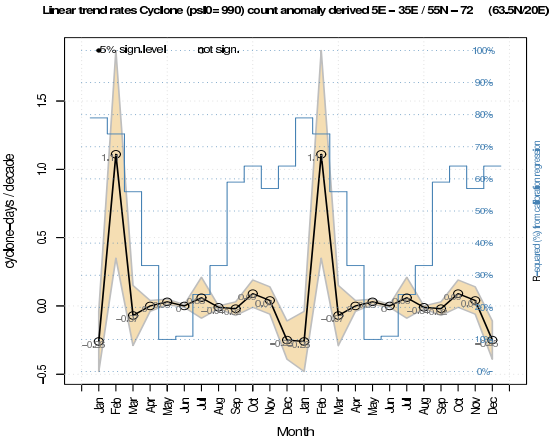

o

p

Figure 5: Figure continued. The results are for GFDL (upper) and NCAR CCSM (lower).

3.3 BCM results

The CCI results for the BCM (T63L16; SRES A2) suggests that the model does not produce sufficiently deep cyclones (Figures 5a,b & 6 – 7). A check of whether the BCM produces realistic SLP structure and magnitudes involved an assessment of the levels, intervals and shape of the SLP contours, shown in Figure 8. Six arbitrary times were selected for the visual inspection of the contours of the absolute SLP values (here in terms of hPa). This additional analysis also indicates a somewhat too weak variability in general. Although trend estimates are indicated on the time series plots, the series are too short to provide reliable trends as the estimates are overly sensitive to year-to-year fluctuations. The annual cycle in the cyclone frequency indicates most pronounced activity in winter, in line with the observations. The deepest cyclones are too few, but are seen in expected regions near the observed storm track in the North Atlantic (Figure 6b,c). The CCI analysis indicates that the BCM generates too many weaker cyclones in the subtropics (Figure 6d).

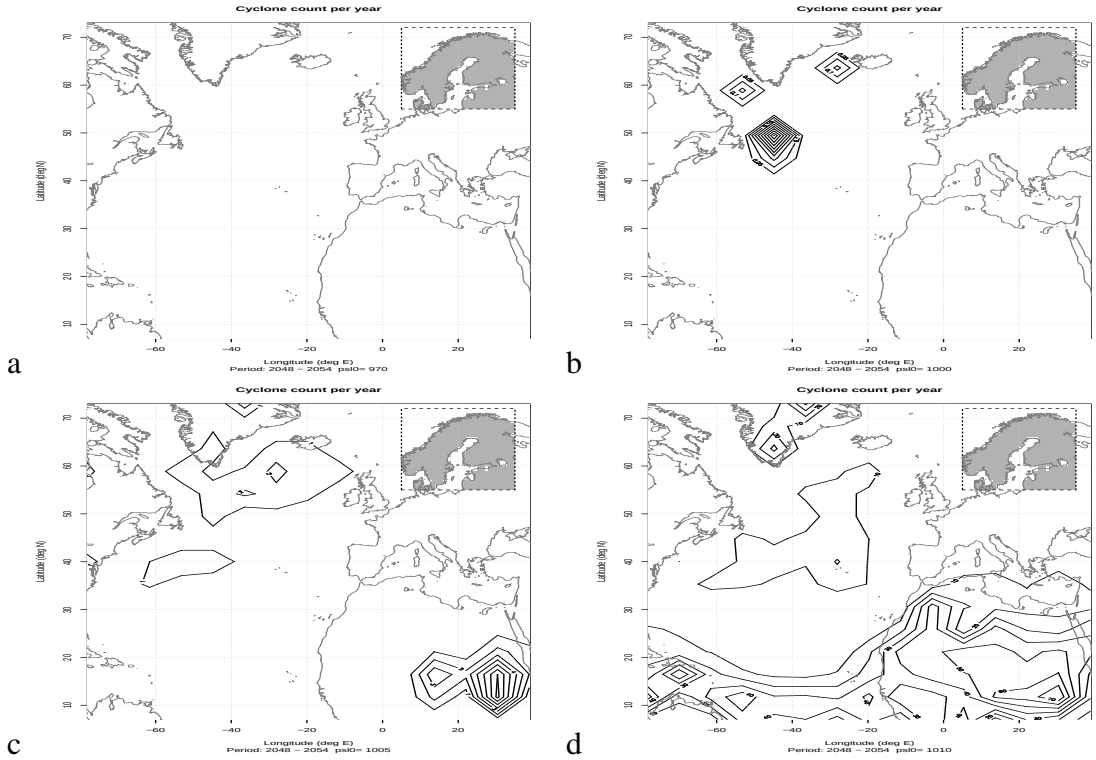

Figure 6: Cyclone statistics from CCI-analysis of BCM-downscaled SLP for the 5°E–35°E/55°N–72°N-region (grey shaded region), following the A2 SRES scenario. Threshold SLP=1000hPa. Threshold SLP are (a) 970hPa, (b), 1000hPa, (c) 1005hPa, and (d) 1010hPa.

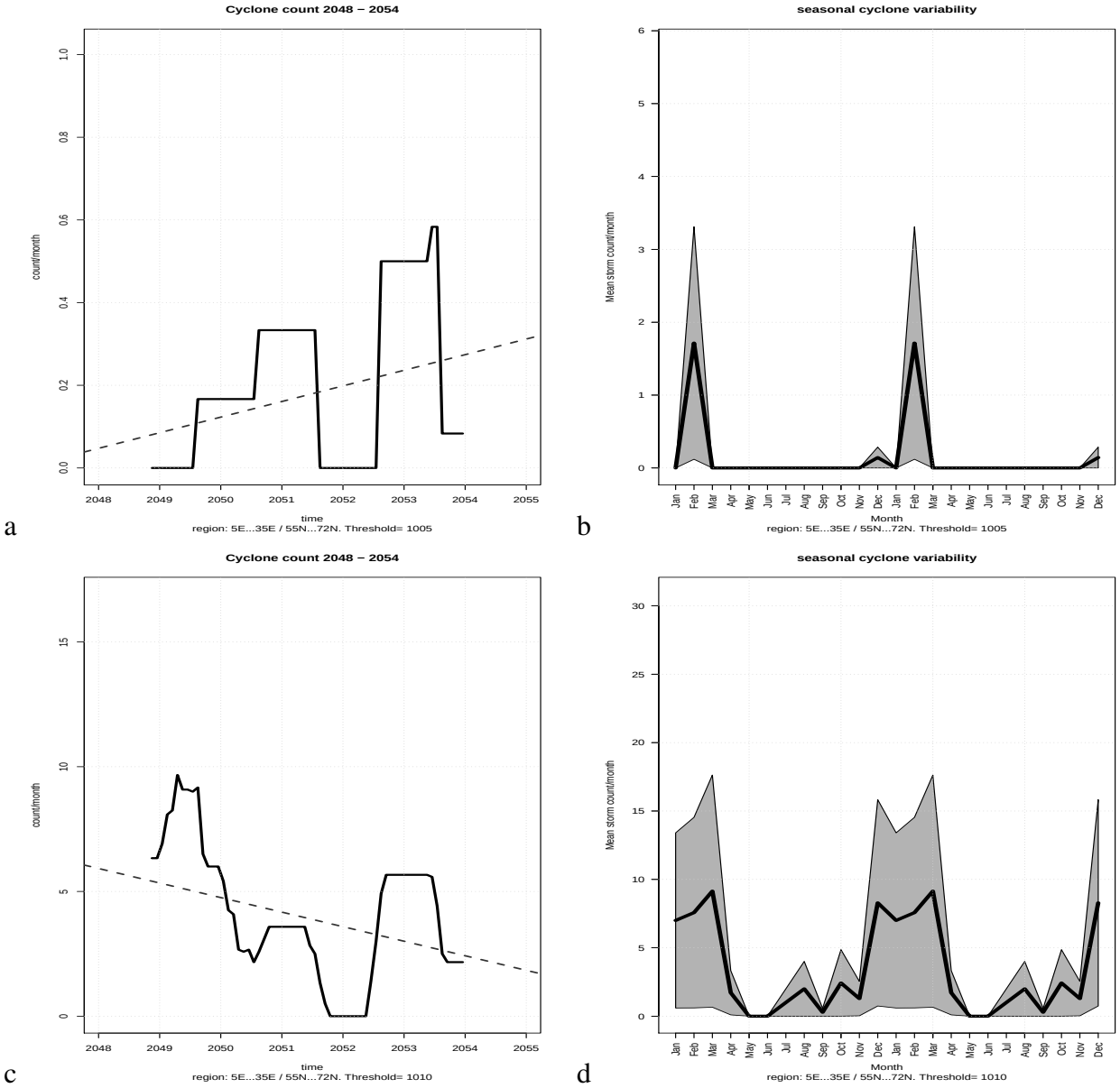

Figure 7: Cyclone statistics from CCI-analysis of BCM-downscaled SLP for the 5°E–35°E/55°N–72°N-region (grey shaded region), following the A2 SRES scenario. Threshold SLP=1000hPa. Threshold SLP are (a–b) 1005hPa, and (c–d) 1010hPa.

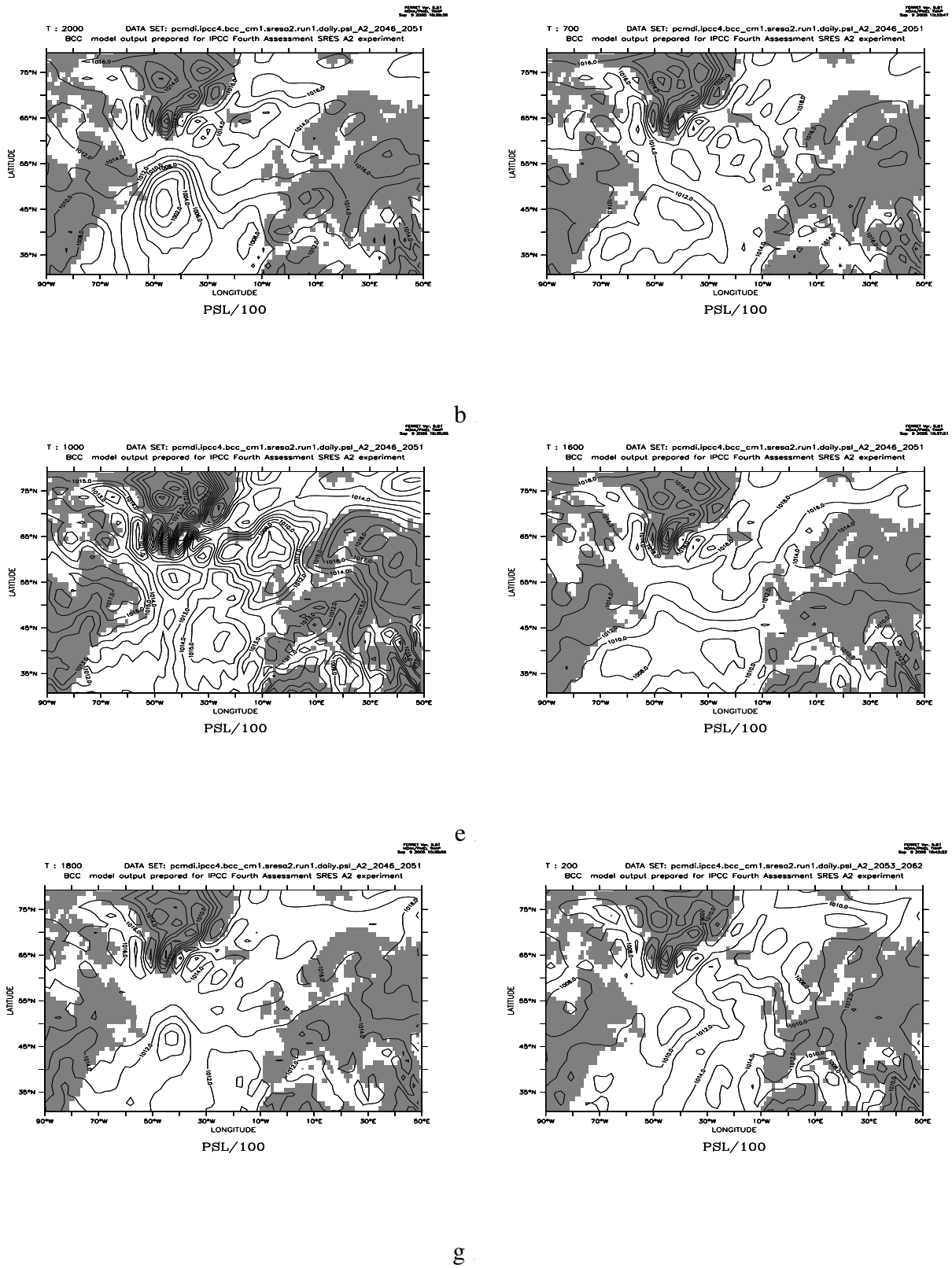

Figure 8: Independent analysis of SLP fields using *Ferret* (http://ferret.pmel.noaa.gov/Ferret/).

3.4 ECHAM5 results

The CCI-analysis was applied to daily SLP from the ECHAM5 model (T63L32; SRES A1b), and the statistics of this analysis are shown in Figure 9. The CCI-analysis of the SLP from ECHAM5 reveal impressively realistic features with high frequency of occurrence in the observed storm track region and with realistic intensities. The number of simulated cyclones deeper than 970hPa is low over Fennoscandia (Figure 9b), however, these storms are rare in the real world and the time series derived here was only 21 years (2081–2101). The one spike in '2086' with value 0.08 counts/month corresponds to a single event (1/12=0.083). In this case, the 'trend' line shown as dashed line gives the impression of a negative 'trend', however, this interpretation is meaningless as this line is derived from one event only.

The representation of slightly more moderate cyclones in ECHAM5 is characterised by more frequent events, that also agree well with the observed storm statistics. The time evolution of the cyclone count (Figure 9b) appear to give an indication of positive trends for those cyclones that are sufficiently frequent to allow for a crude trend analysis. However, the time series are too short to provide reliable estimates and the trend estimates are sensitive to year-to-year fluctuations.

The simulated seasonality of the cyclones is furthermore realistic in ECHAM5 (Figure 9g–i). The strongest cyclones tend to be confined to the winter season (g), whereas weaker cyclones are almost as frequent in summer as in winter (i).

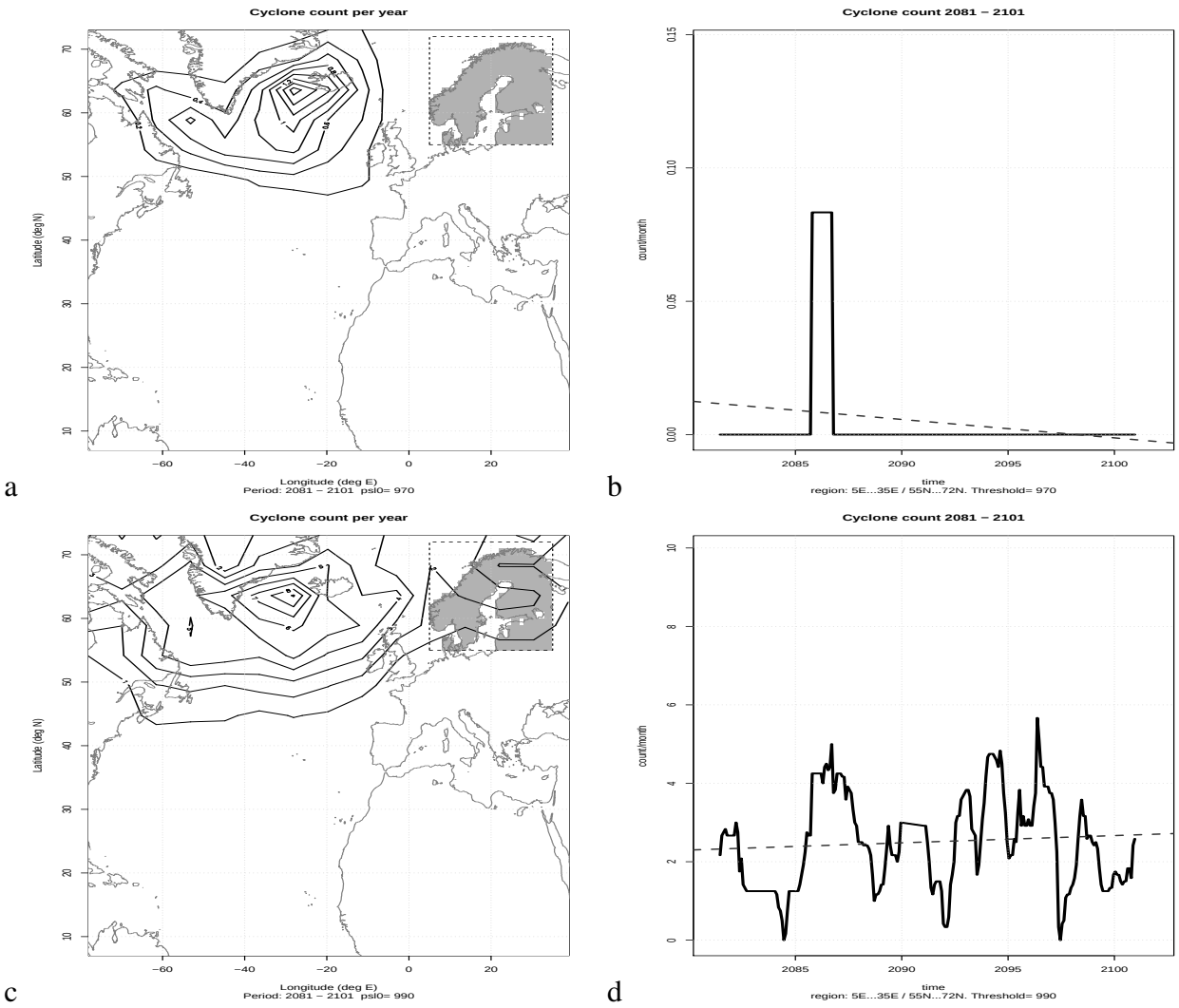

Figure 9: Cyclone statistics from CCI-analysis of ECHAM5 for the 5°E–35°E/55°N–72°N-region (grey shaded region), following A1b SRES scenario. Threshold SLP=970hPa for panels a–b and 990 for panels c–d.

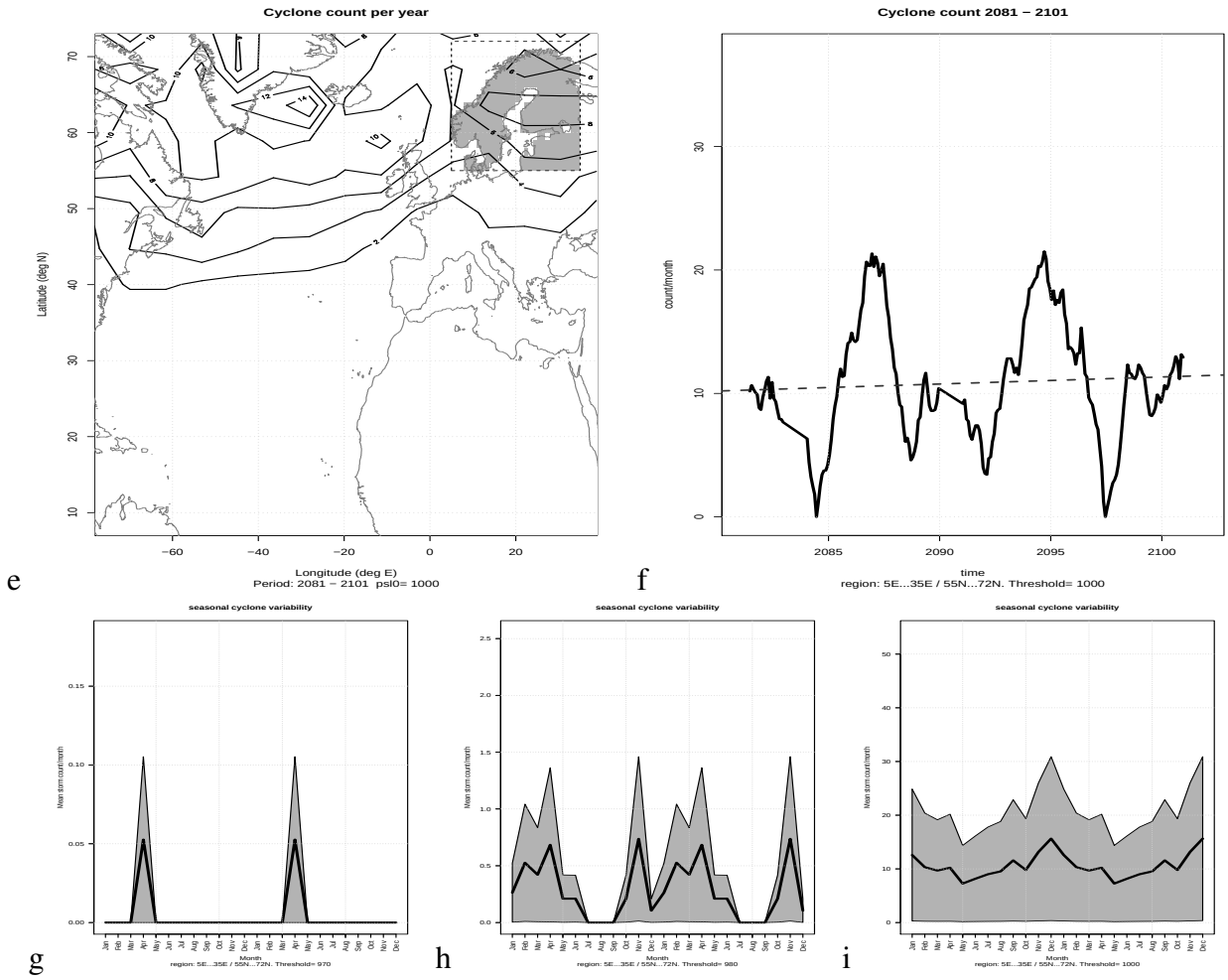

Figure 9: Figure continued: Cyclone statistics from CCI-analysis of ECHAM5 SLP for the 5°E–35°E/55°N–72°N-region (grey shaded region). Threshold SLP=1000hPa for panels e–f and the seasonal variations for thresholds 970, 980, and 1000 hPa in panels g–i.

4 Dynamically downscaled results

The preliminary analysis presented in Figures 6–9 suggest that state-of-the-art GCMs are able to provide a reasonably accurate description on mid-latitude storms. One possible reason for why GCMs in general, and BCM in particular, may not capture the range of central pressure levels (storm intensity) associated with the storms is that the spatial resolution of the GCMs (typically 200km) may be too coarse for a proper cyclone representation, however the ECHAM5 model has the same spatial horizontal resolution (T63L32) as the BCM (T63L16) and does give a realistic description of the cyclone statistics. The two models differ in their vertical resolution, with 32 different vertical levels in the ECHAM5 and only 16 in BCM. The CCI-analysis was therefore repeated for dynamically downscaled results (typically 50km) in order to see if the general character of the cyclone statistics were sensitive to the spatial resolution.

4.1 Downscaled met.no/HadCM3 cyclone statistics

Figure 10 shows the results derived using HIRHAM to downscale HadCM3. The RCM yields a realistic representation of highest cyclone frequencies in the storm track region near Iceland. The number of years analysed here is too low to allow an analysis of the time evolution. Furthermore, the number of cyclones with central pressure deeper than 990hPa is very low (Figure 10b). Hence a trend analysis is not possible for this case. There appears to be an indication of a slight decline in the number of weaker cyclones over time (f), however, the series on which these annual variations were short which means that the annual estimates are sensitive to sampling fluctuations. The annual variability in the cyclone number is realistic with a winter-time peak.

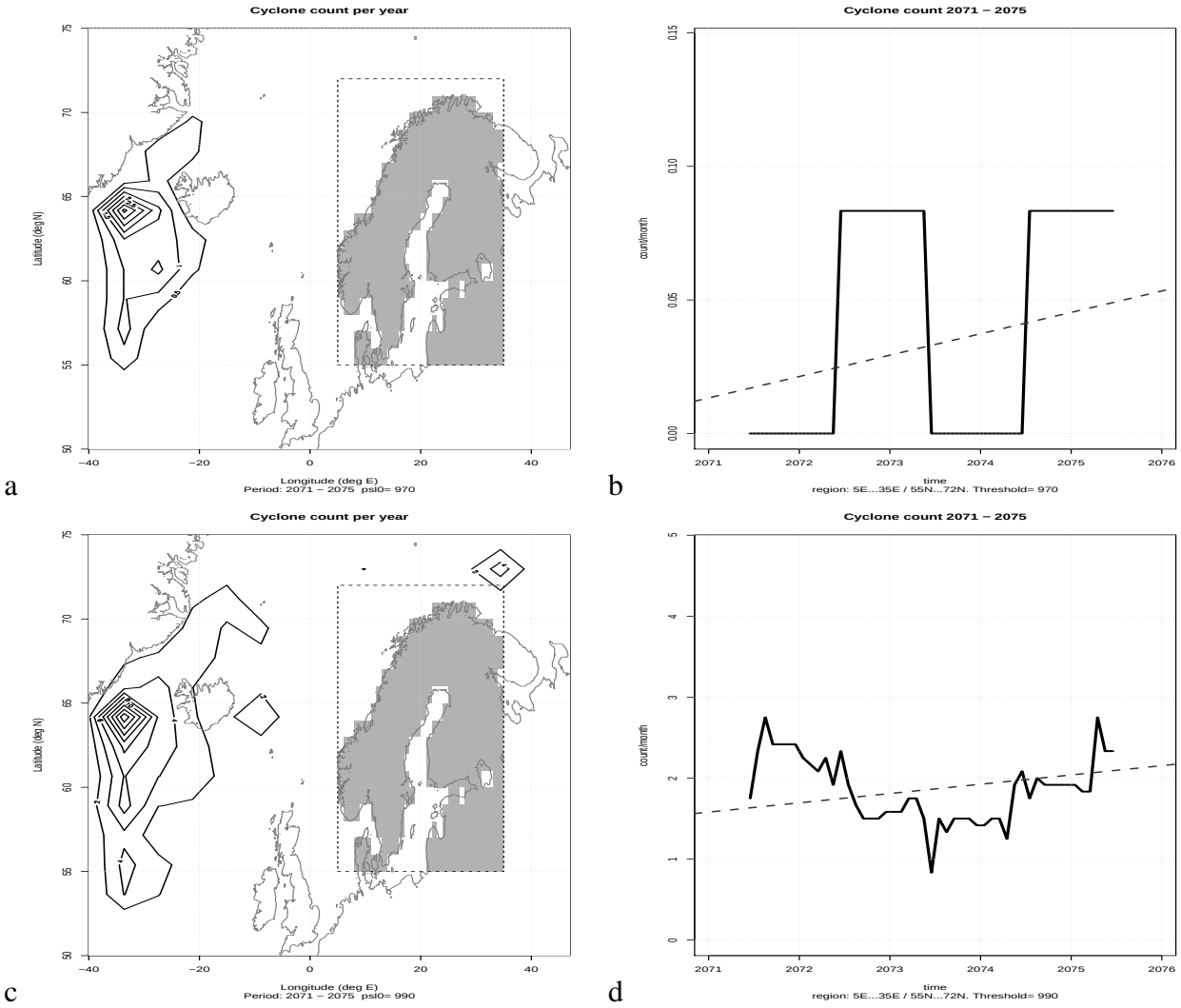

Figure 10: Cyclone statistics from CCI-analysis of HIRHAM-downscaled SLP, driven by the global HadCM3 A2 SRES scenario. Threshold SLP=970hPa for panels a–b and 990 for panels c–d.

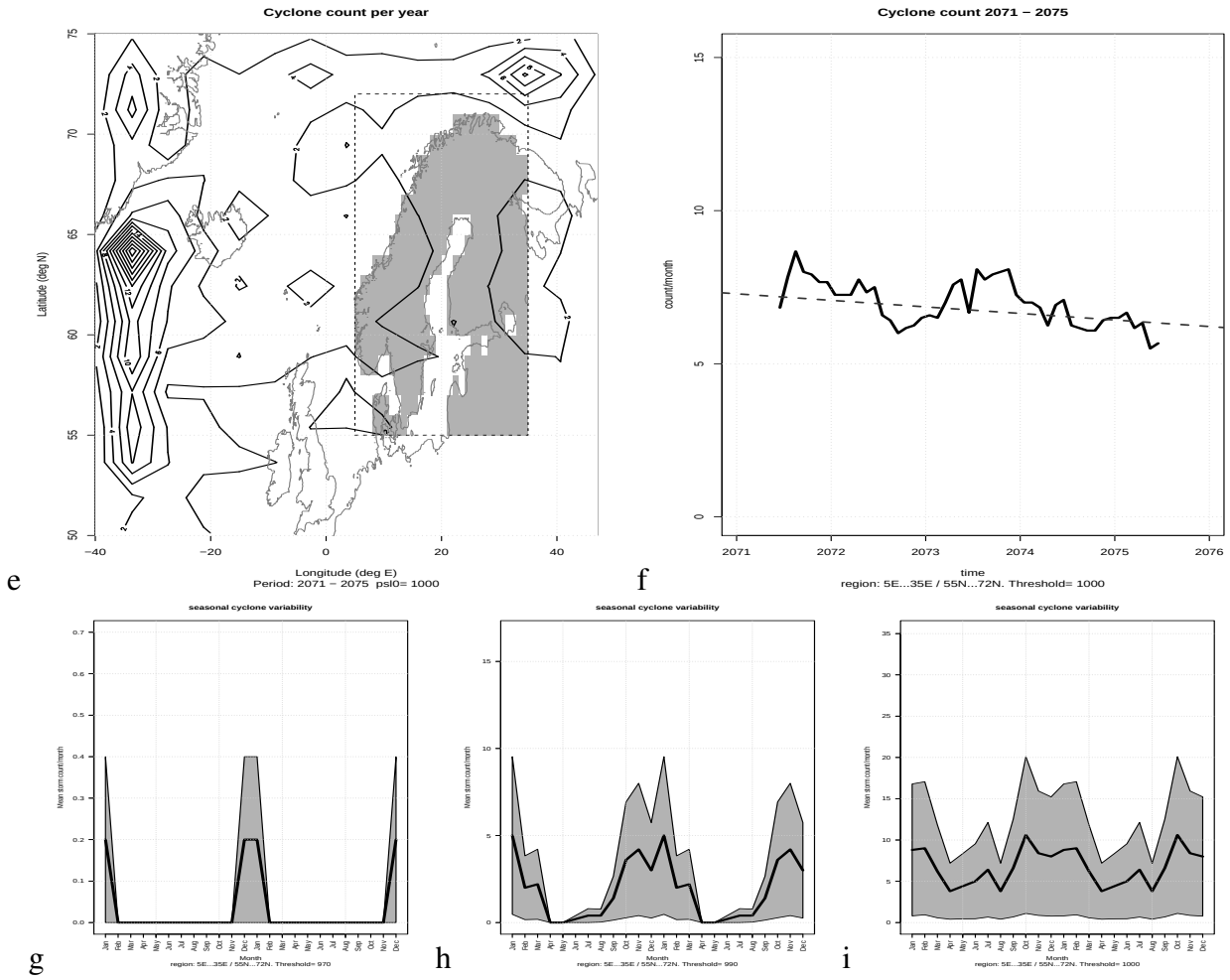

Figure 10: Figure continued: Cyclone statistics from CCI-analysis of HIRHAM-downscaled SLP, driven by the global HadCM3 A2 SRES scenario. Threshold SLP=1000hPa for panels e–f and the seasonal variations for thresholds 970, 990, and 1000 hPa in panels g–i.

4.1.1 Downscaled DMI/PRUDENCE cyclone statistics

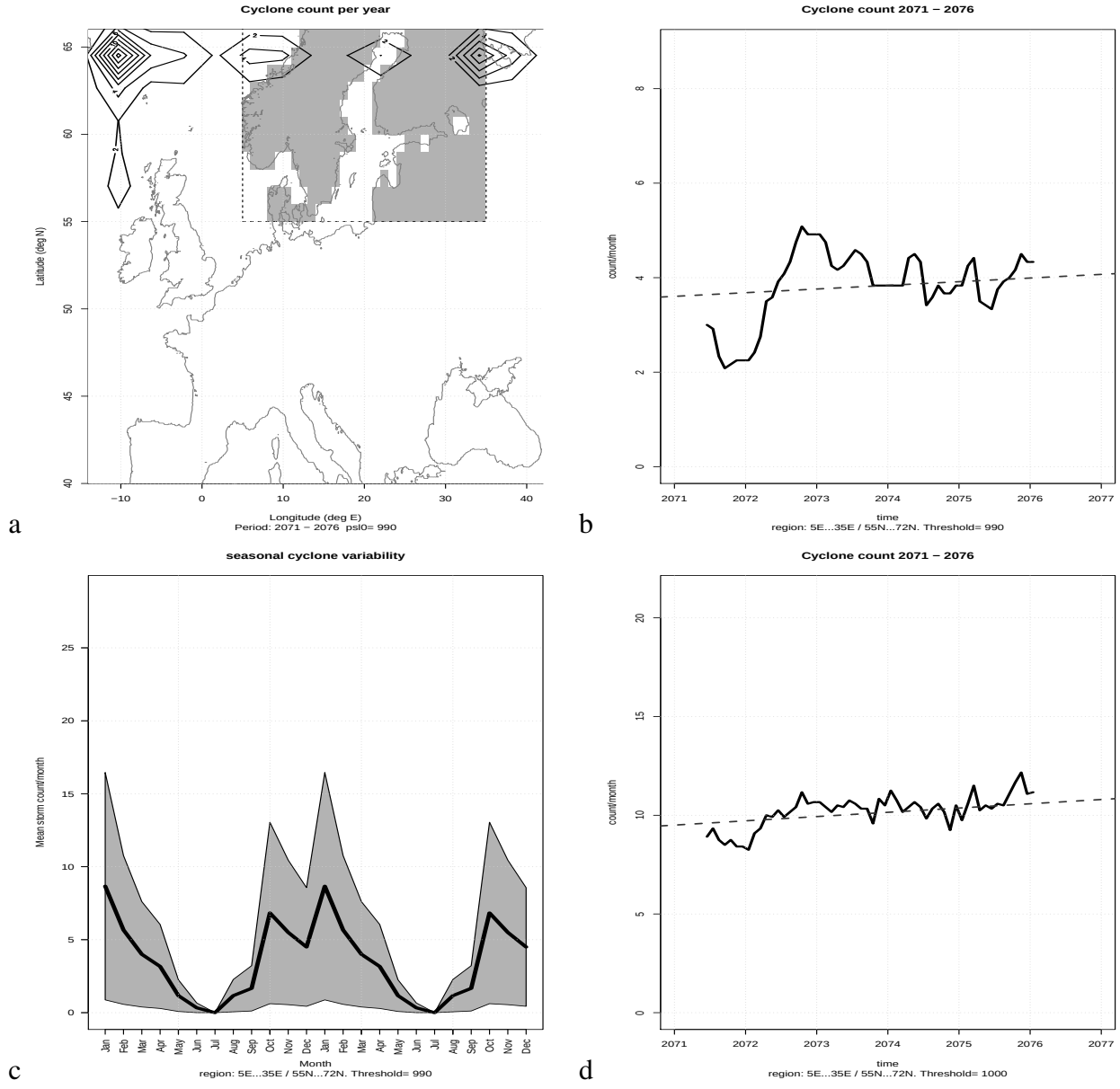

Figure 11: Cyclone statistics from CCI-analysis of DMI-downscaled SLP (HIRHAM, PRUDENCE), driven by the global ECHAM5 A2 SRES scenario. Threshold SLP=970hPa for panels a–c and 990 for panel d.

The CCI-analysis was applied to dynamically downscaled results based on the DMI high-resolution RCM (25×25 km^2) and the results are shown in Figure 11. Since the domain used by the RCM did not cover most of the storm track area, it is difficult to assess the degree of realism in the geographical distribution of the storms. The annual cycle is realistic (Figure 11c), although the apparent double-peak feature may be due to the short time series. The short record makes a trend analysis very uncertain, and it is not possible to say whether the apparent slightly upward trend is part of a systematic increase or due to decadal undulations.

5 Extrapolation of trends of deep & rare cyclones.

It is notoriously difficult to estimate trends in very rare events (*IPCC*, 2002) since it usually is impossible to get a sufficiently large sample. However, if a number of assumptions are made, it may be possible to make some 'educated guesses'. Constraints may set lower and upper limits, as there are physical limits to how deep the cyclones get and weaker cyclones are frequent. Here we will impose a lower limit for the central storm pressure, although this will be significantly higher than the physical limit, as we will use empirical-based values from historical data. It will be assumed that the trend in cyclone statistics will change smoothly with the central pressure - imposing a slow manifold that converges to zero at a lower threshold value. Then, trends can be estimated for moderately intense cyclones, for which the number is sufficiently high to yield a reasonable estimate, and the values for more powerful storms can be inferred by means of extrapolation from the weaker cyclones under a convergence to zero for very low central pressures.

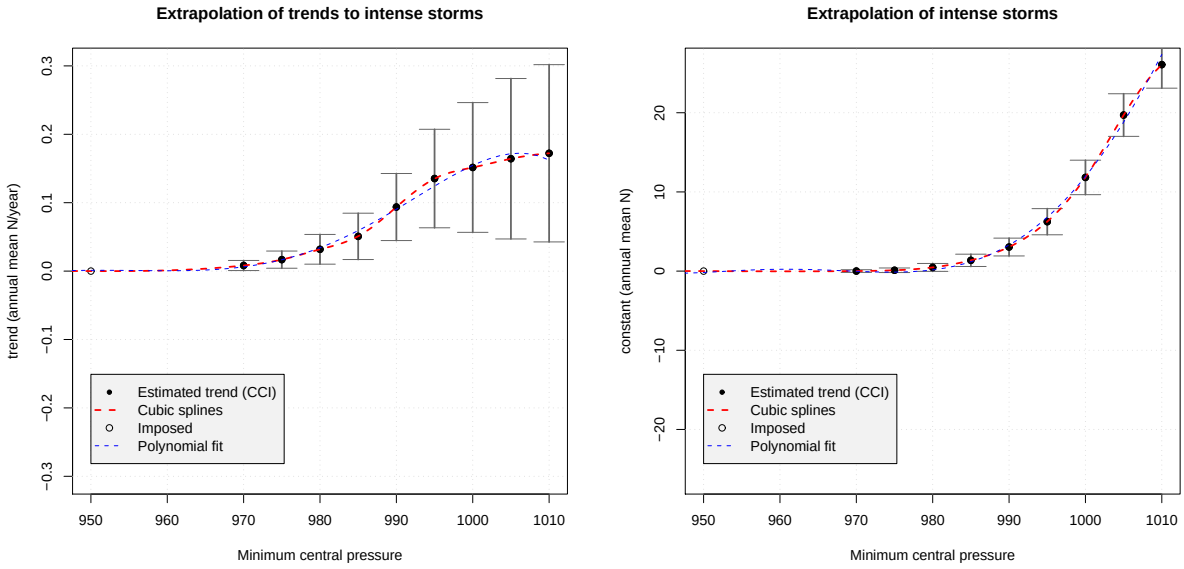

Figure 12: The dependency of storm trend estimates to threshold value for central pressure. A cubic spline interpolation (red curve) is used to interpolate between the empirical estimates obtained using NMC gridded historical analysis and imposed zero-trend for 950hPa (assuming no storms reaching this intensity). Left panel shows estimates for β (rate of change) in the linear trend model $N = \alpha + \beta t$, and the right panels show α (constant).

Figures 12–15 show the structure of the trend analysis for historical cyclones over the 5°E–35°E/55°N–72°N-region, derived from the NMC and the ERA40 data. The estimates are shown as black symbols with error bars ($\pm$ 2 $\times$ st.dev.), and the red lines show cubic spline interpolations, with an imposed zero value at 950hPa. Both these analysis indicate positive trends in the storm frequency over the last $\sim$40 years. The error bars associated with the trend estimates suggest that these are statistically significant.

The blue curves shown in Figures 12–22 represent polynomial fits to the frequency-pressure structures, and the estimated coefficients for the fits to the historical data and ECHAM5 are provided in the Appendix. The appendix also provides tables of the best estimates of linear trends and coefficients for similar empirical models ($N = \alpha + \beta t$, where t is taken as $t = 1 \cdots$length of series [number of years]) as those shown in Figure 23, but for different threshold pressures.

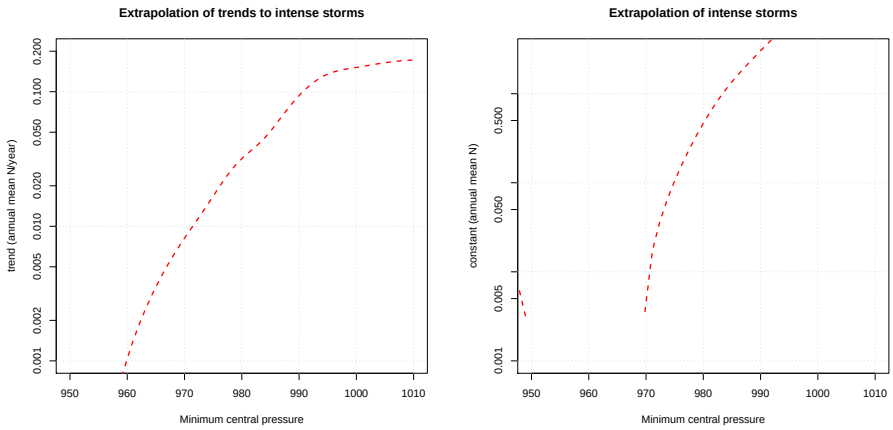

Figure 13: Same as Figure 12, but with a logarithmic ordinate.

Figures 16–17 show similar extrapolations derived from the ECHAM5 model scenarios for model years 2081–2101. The analysed series is too short to provide significant results, and the error bars enclose the zero-line. The same analysis applied to the BCM (Figure 18–19), however, was hampered by too few cyclones which were unrealistically weak. The same analysis applied to downscaled results with HIRHAM (Figures 20–21) were considered unreliable as a result of too short intervals for reliable trend estimates, however, the RCM did seem to reproduce cyclones with realistic intensities.

Figure 23 shows a synthesis plot of the results derived from the simple linear trend models for the cyclone frequency (number of cyclones in 5°E–35°E/55°N–72°N) for threshold central pressures of 970hPa (a) and 980hPa (b). The uncertainty associated with these estimates are manifested as differences between the different curves. For historical trends, the NMC data (black) yields a higher number of cyclones than the ERA40 (grey), however, it is reasonable to believe that the ERA40-estimates are more reliable than the older NMC. The historical analyses indicate linear trends, if persisting, would yield higher cyclone frequencies than obtained by CCI applied to model simulations for the future. The BCM (red) appears to under-estimate the number of cyclones whereas both the ECHAM5 model (dark red) and HIRHAM (green) describe a frequency that is consistent with the range of the ERA40 trend model for the historical observations (solid grey line). However, the estimates derived from ECHAM5 and HIRHAM are substantially lower than the extrapolation of the historical ERA40 trends to the future (dashed grey line). The DMI with a higher spatial resolution projects increased level of cyclone frequency.

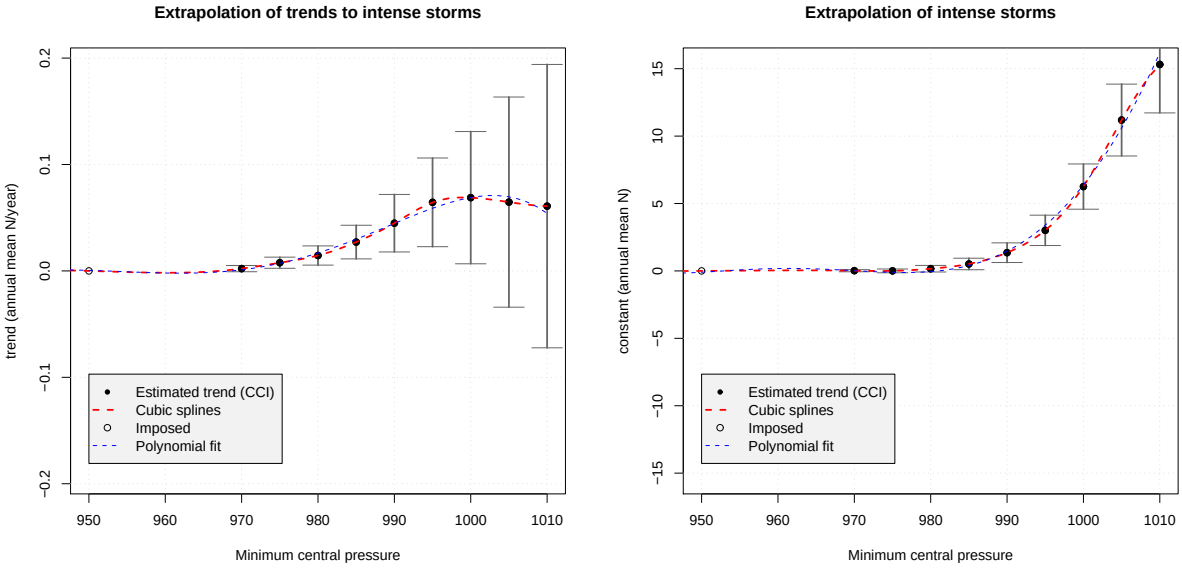

Figure 14: The dependency of storm trend estimates to threshold value for central pressure. A cubic spline interpolation (red curve) is used to interpolate between the empirical estimates obtained using ERA40 reanalysis and imposed zero-trend for 950hPa (assuming no storms reaching this intensity). Left panel shows estimates for β (rate of change) in the linear trend model $N = \alpha + \beta t$, and the right panels show α (constant).

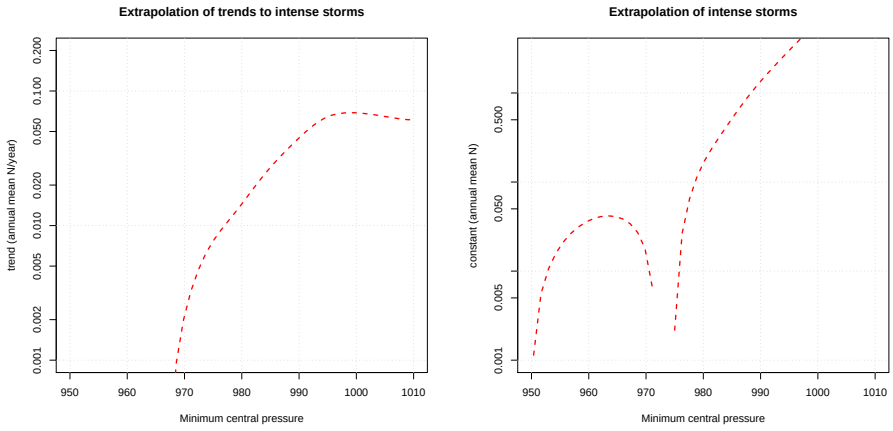

Figure 15: Same as Figure 14, but with a logarithmic ordinate.

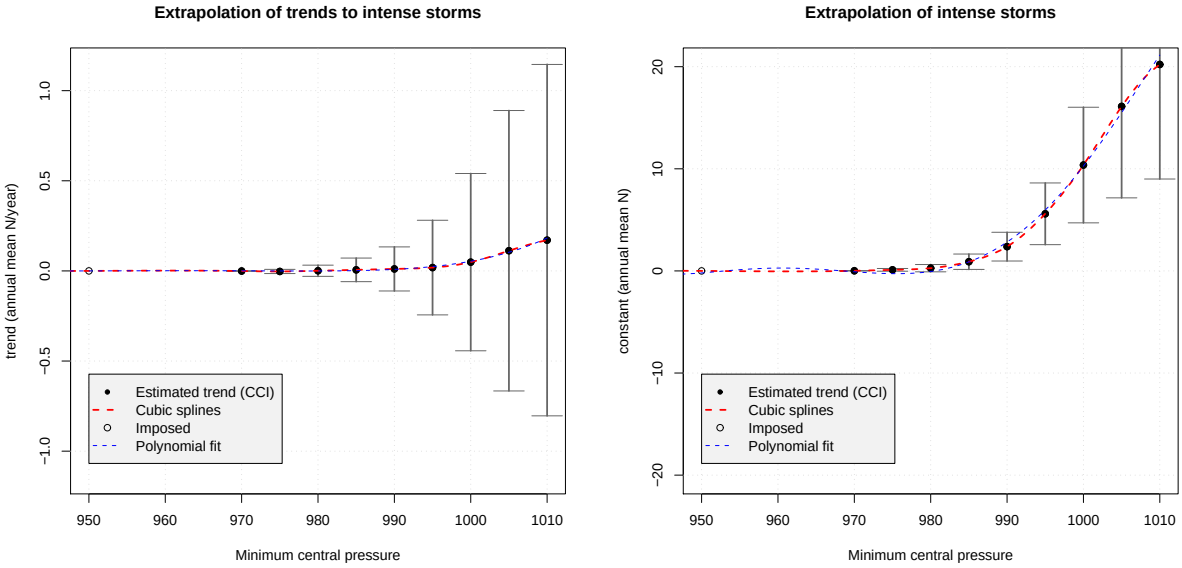

Figure 16: The dependency of storm trend estimates to threshold value for central pressure. A cubic spline interpolation (red curve) is used to interpolate between the empirical estimates obtained using ECHAM5 and imposed zero-trend for 950hPa (assuming no storms reaching this intensity). Left panel shows estimates for β (rate of change) in the linear trend model $N = \alpha + \beta t$, and the right panels show α (constant).

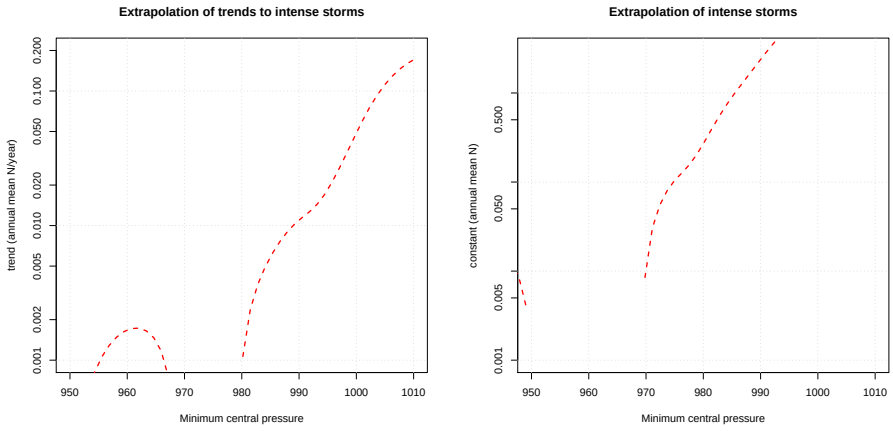

Figure 17: Same as Figure 14, but with a logarithmic ordinate.

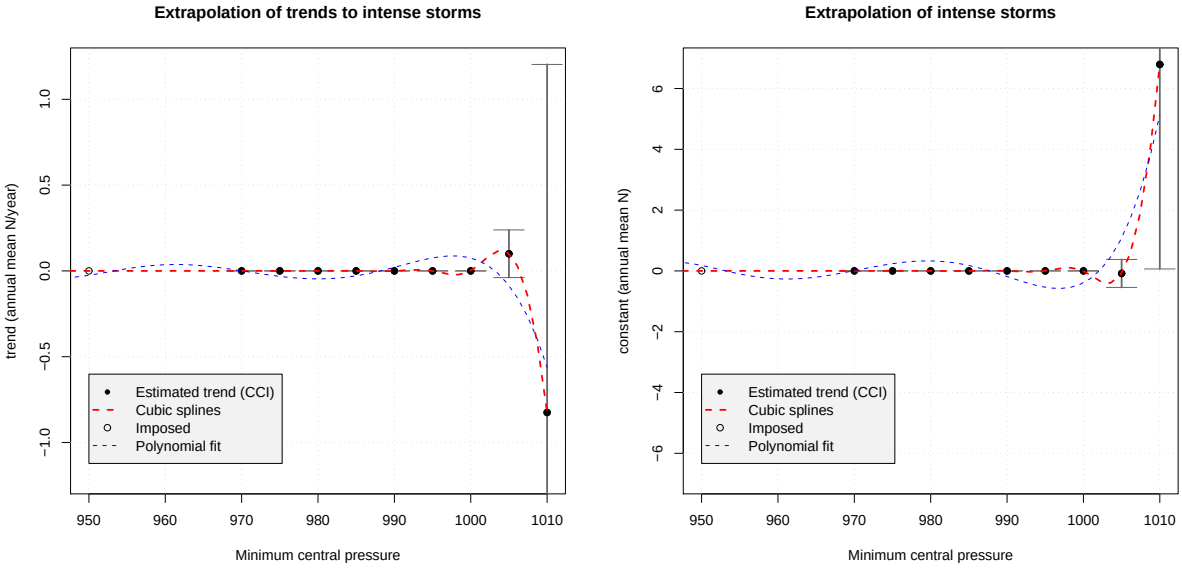

Figure 18: The dependency of storm trend estimates to threshold value for central pressure. A cubic spline interpolation (red curve) is used to interpolate between the empirical estimates obtained using BCM (SRES A2) and imposed zero-trend for 950hPa (assuming no storms reaching this intensity). Left panel shows estimates for β (rate of change) in the linear trend model $N = \alpha + \beta t$, and the right panels show α (constant).

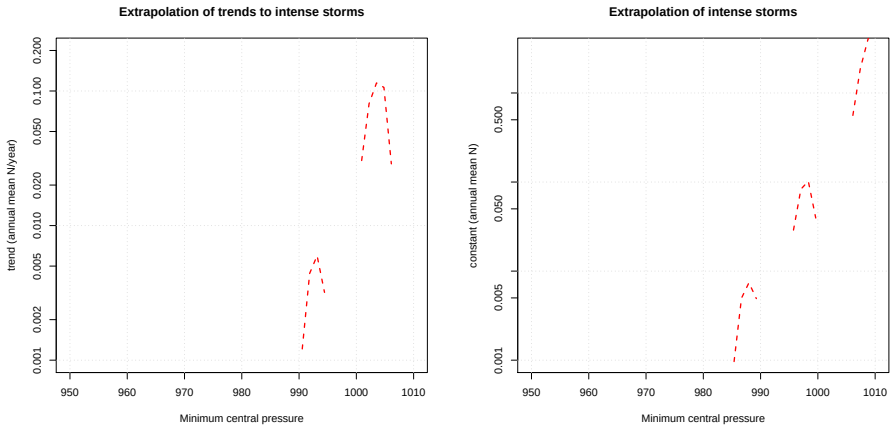

Figure 19: Same as Figure 18, but with a logarithmic ordinate.

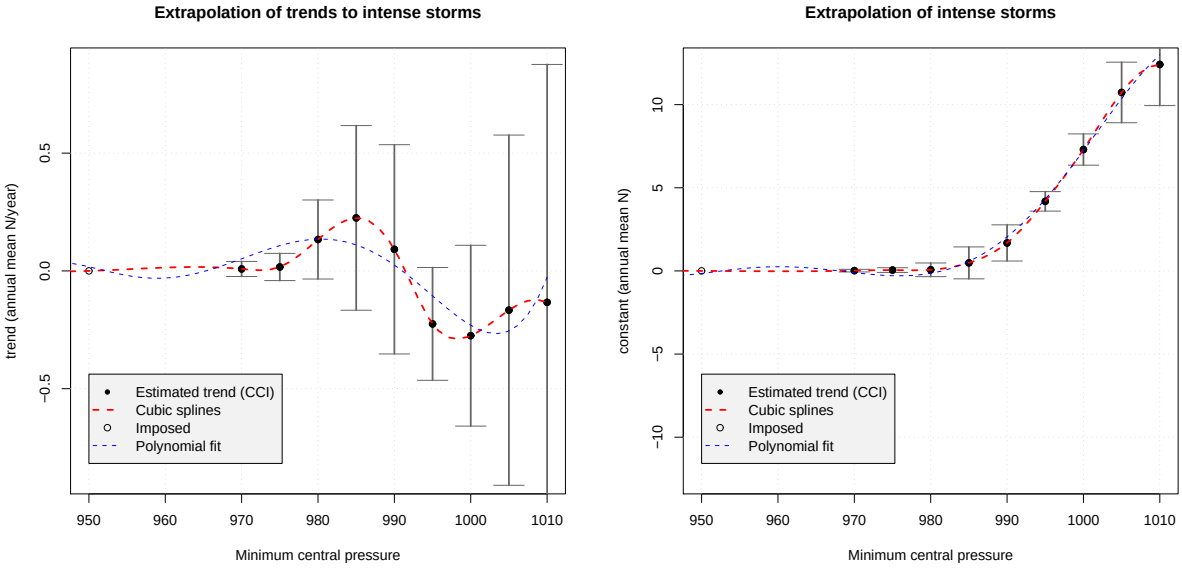

Figure 20: The dependency of storm trend estimates to threshold value for central pressure. A cubic spline interpolation (red curve) is used to interpolate between the empirical estimates obtained using dynamically downscaled values (HIRHAM SRES A2) and imposed zero-trend for 950hPa (assuming no storms reaching this intensity). Left panel shows estimates for β (rate of change) in the linear trend model $N = \alpha + \beta t$, and the right panels show α (constant).

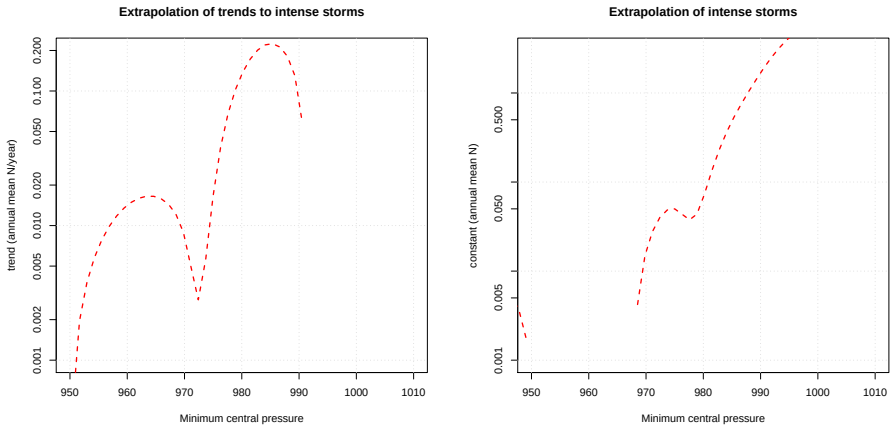

Figure 21: Same as Figure 20, but with a logarithmic ordinate.

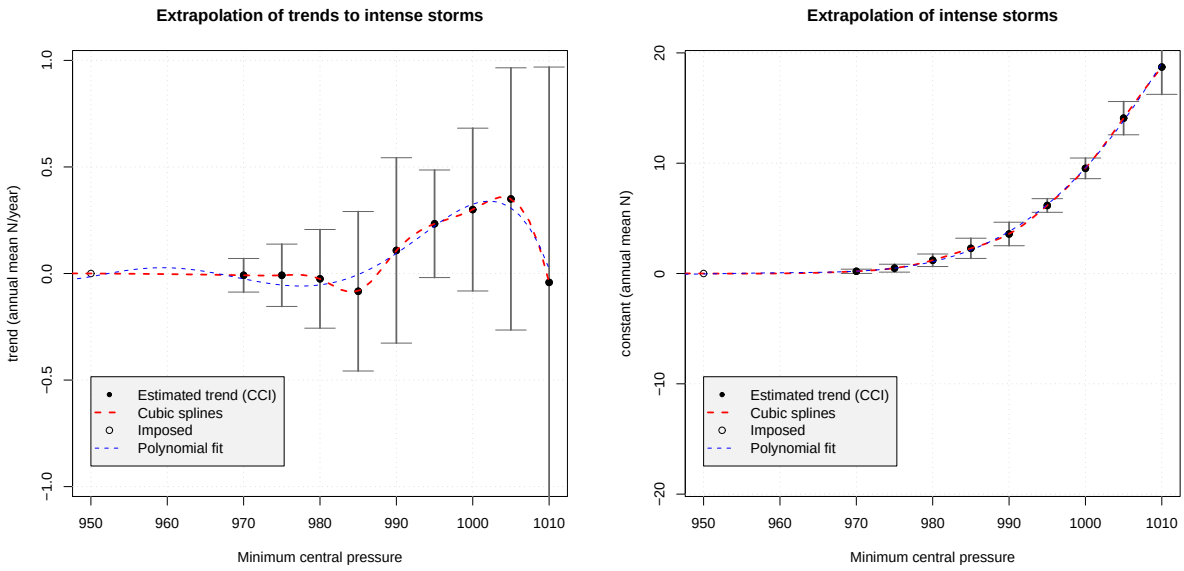

Figure 22: The dependency of storm trend estimates to threshold value for central pressure. A cubic spline interpolation (red curve) is used to interpolate between the empirical estimates obtained using dynamically downscaled values (DMI SRES A2) and imposed zero-trend for 950hPa (assuming no storms reaching this intensity). Left panel shows estimates for β (rate of change) in the linear trend model $N = \alpha + \beta t$, and the right panels show α (constant).

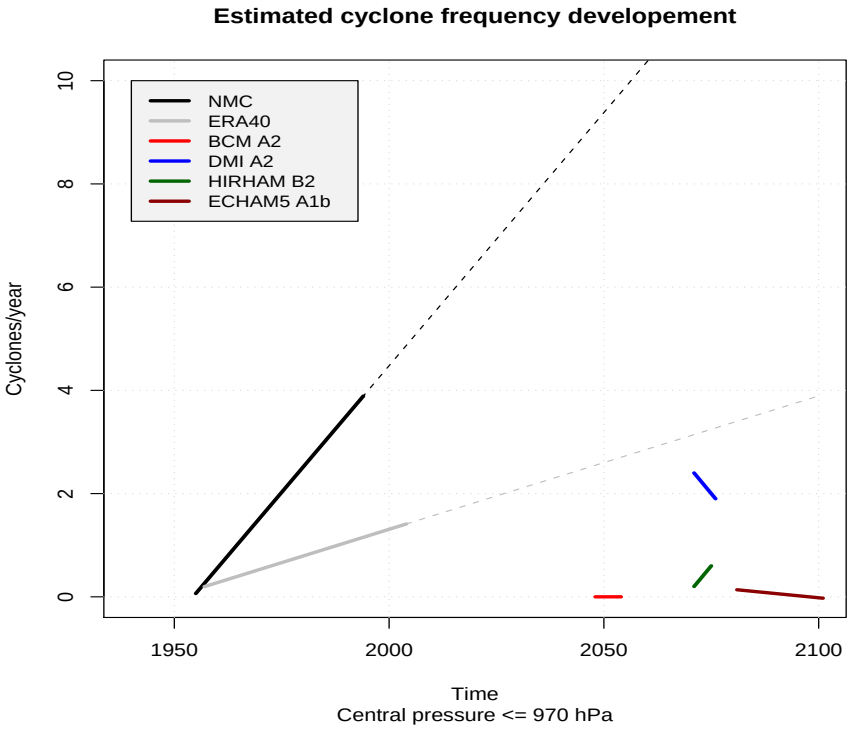

a

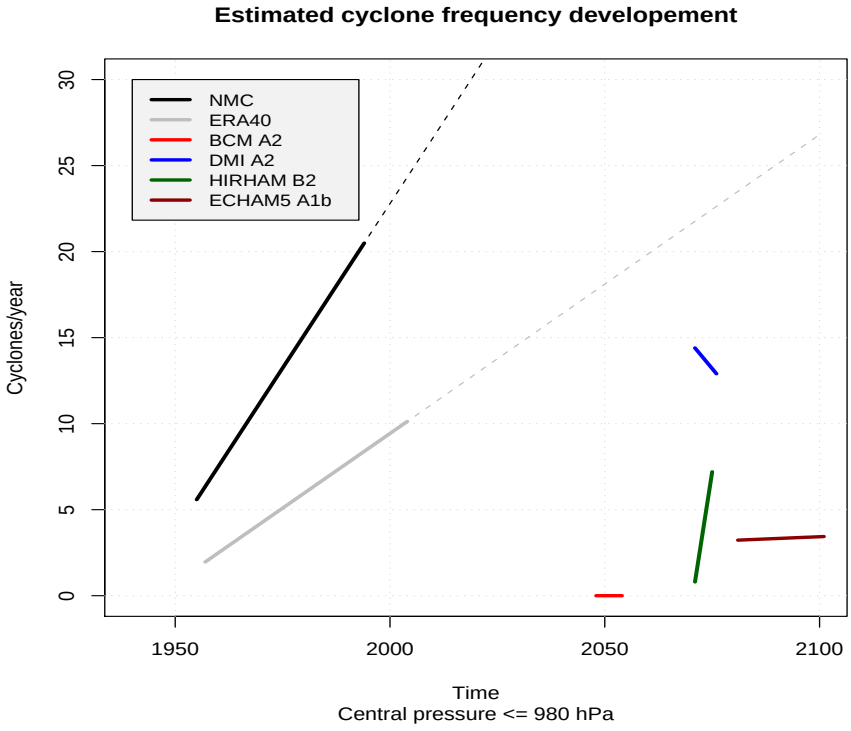

b

Figure 23: A synthesis of historical trends and projections of number of cyclones in 5°E–35°E/55°N–72°N, based on estimates from the analyses shown in Figures 12–21. (a) threshold pressure of 970hPa, (b) threshold pressure of 980hPa.

6 Discussion & Conclusions

One major caveat of this analysis is the fact that all the GCM/RCM-CCI analyses involved really are too short time series to make firm conclusions about the future development. Hence, these results must be regarded as sketchy best guesses at this stage. Longer time series will reduce this uncertainty.

The CCI results for historical Atlantic mid-latitude cyclones suggest that there has been an increasing trend in the number of storms over the last 40–50 years. This observation is consistent with the findings by *Geng & Sugi* (2001) analysed the NCEP reanalysis over the upwind region 45°N–80°N/80°W–0°E (different data product, but based on much the same underlying observations). It is likely that the observed increase may be caused by a shift in storm track location, as *Smits & Können* (2005) reported reduced storminess over the Netherlands over the 1962–2002 period.

Statistical modelling based on large-scale SLP point does not suggest any systematic trend that is common amongst the different climate models. This result is in agreement with earlier SLP-based analysis, but for precipitation (*Benestad*, 2002) rather than cyclones. A local trend in the SLP would imply a systematic redistribution of the atmospheric mass over that region, given a stable state. However, a systematic change in the frequency of low-pressure systems afflicting a given region could also manifest itself as a change in the local mean SLP. It is believed that for these reasons, a statistical downscaling approach is not a suitable method for analysing cyclone trends.

Here the region covering 5°E–35°E/55°N–72°N was chosen for estimating the cyclone frequency. A smaller region will imply greater uncertainty, due to lower number of events within its boundaries and thus a larger sampling fluctuations. If storm frequency is required for a smaller region, a simple way to estimate the frequency is to scale the numbers presented here with the ratio of the area of the region of interest to that of 5°E–35°E/55°N–72°N.

It is almost impossible to estimate trends for rare extreme events due to large sampling fluctuations and few data points. Analysis of very rare deep cyclones based on series whose length is shorter than their average return interval is not possible as the occurrence of these events has a random character to a large degree. One can nevertheless postulate - a physically plausible proposition - that the trend in number of cyclones deeper than a given threshold value varies smoothly with the threshold central pressure. Therefore, a preferable approach is to estimate the behaviour of the rare storms through an extrapolation based on the trends in more frequent and weaker storms, albeit this approach is still associated with high uncertainties. Moreover, if one assumes that the trend is a smooth function of the severity of the event, i.e. a threshold value, then it is possible to make a crude extrapolation based on the estimates for more frequent and less severe events, assuming that that the number of events beyond a given upper limit for physically realistic central pressure can be approximated to zero, and thus imposing a zero trend at for very intense hypothetical events (one can also use model based estimates for what is actually physically possible). Figure 23 shows the trends estimated for the observed central pressure of the past and future derived from the cubic spline interpolations giving estimates for other threshold values in Figures 12–22 where a zero-trend was imposed for central pressures below 950hPa.

Figure 23 can serve as a tentative guidance for projecting future cyclone frequencies. The results presented here can indicate that future cyclone frequencies may be higher than historical levels. A likely guestimate for the upper limit on the cyclone frequency can be taken as the dashed grey line (ERA40),

It is expected that GCMs will improve in the future with higher spatial resolution and better representation

of cyclones. Therefore, these results should be regarded as tentative at present stage, which will probably be followed by less uncertain analysis in the future.

Acknowledgement

This work was supported by Skogforsk, but was also based on previous work done under the Norwegian Regional Climate Development under Global Warming (RegClim) programme, and was supported by the Norwegian Research Council (Contract NRC-No. 120656/720) and the Norwegian Meteorological Institute. I acknowledge the international modeling groups for providing their data for analysis, the Program for Climate Model Diagnosis and Intercomparison (PCMDI) for collecting and archiving the model data, the JSC/CLIVAR Working Group on Coupled Modelling (WGCM) and their Coupled Model Intercomparison Project (CMIP) and Climate Simulation Panel for organizing the model data analysis activity, and the IPCC WG1 TSU for technical support. The IPCC Data Archive at Lawrence Livermore National Laboratory is supported by the Office of Science, U.S. Department of Energy.

Table 2: Abbreviations

A1b	A particular SRES emission scenario.
CCI	Calculus-based Cyclone Identification
CCSM	GCM from NCAR (*Blackmon* et al., 2001)
DMI	Dansih Meteorological Institute (www.dmi.dk)
ECHAM5	GCM from Max-Planck-Institute, Germany (*Giorgetta* et al., 2002)
ECMWF	European Centre for Medium-range Weather Forecasts
ERA40	40-year re-analysis from ECMWF
GCM	Global Climate Model
GFDL	GCM from Geophysical Fluid Dynamics Lab (*Delworth* et al., 1999)
GIN	Greenland Iceland Norwegian [Sea]
HadCM3	GCM from UK MetOffice (*Gordon* et al., 2000)
HadCEM1	Most recent GCM from UK MetOffice.
HIRHAM	RCM from met.no/DMI (*Christensen* et al., 1996).
hPa	hecto-Pascal (SI units: $100Nm^{-2}$)
IPCC	Intergovernmental Panel on Climate Change
met.no	The Norwegian Meteorological Institute (www.met.no)
NCAR	National Center for Atmospheric Research, USA
NMC	National Meteorological Center (now NCEP)
NCEP	National Center for Environmental Prediction (USA)
PCMDI	Program for Climate Model Diagnosis and Intercomparison
RCM	Regional Climate Model
SLP	Sea Level Pressure
SRES	Special Report Emission Scenarios
T63L16	Spectral resolution (number of harmonics): triangular 63, 16 vertical levels.
T63L32	Spectral resolution (number of harmonics): triangular 63, 32 vertical levels.

Appendix

	NMC					
y	c	a_1	a_2	a_3	a_4	a_5
α	(4.509±2.716)×10^{-1}	(-2.677±0.809)×10^{-1}	(3.212±0.733)×10^{-2}	(-1.379±0.268)×10^{-3}	(2.305±0.423)×10^{-5}	(-1.142±0.241)×10^{-7}
β	(-0.731±3.350)×10^{-3}	(0.869±9.979)×10^{-4}	(4.649±9.040)×10^{-5}	(-5.229±3.308)×10^{-6}	(1.702±0.523)×10^{-7}	(-1.407±0.297)×10^{-9}
	ERA40					
y	c	a_1	a_2	a_3	a_4	a_5
α	(2.541±1.751)×10^{-1}	(-1.557±0.522)×10^{-1}	(1.853±0.4725)×10^{-2}	(-7.656±1.729)×10^{-4}	(1.200±0.273)×10^{-5}	(-5.331±1.554)×10^{-8}
β	(-0.6.78±1.735)×10^{-3}	(5.396±5.168)×10^{-4}	(-4.805±4.681)×10^{-5}	(0.228±1.713)×10^{-6}	(4.341±2.707)×10^{-8}	(-5.164±1.539)×10^{-10}
	ECHAM5	2081–2101				
y	c	a_1	a_2	a_3	a_4	a_5
α	(5.334±2.402)×10^{-1}	(-3.243±0.716))×10^{-1}	(3.975±0.648)×10^{-2}	(-1.752±0.237)×10^{-3}	(3.055±0.375)×10^{-5}	(-1.691±0.213)×10^{-7}
β	(-0.097±2.645)×10^{-3}	(-0.791±7.879)×10^{-4}	(0.695±7.138)×10^{-5}	(0.530±2.612)×10^{-6}	(-3.689±4.128)×10^{-8}	(5.103±2.347)×10^{-10}

Table 3: Empirical models for approximate values for the dependency of number of cyclones per month (N)as a function of central pressure depth p_0: $N = \alpha + \beta t$, where α and β can be approximated by $y = c + \sum_{i=1}^{5}(a_i x^i)$ and $0 \geq x \geq 50$. Here x is taken as $p_0 - 940$ (units hPa). Figures are given with $\pm$ one standard error. Large errors indicate that the 5th-order polynomial does not give a good match with the structure of regression coefficients' dependence to minimum central pressure.

NMC

psl	const	slope
940	0	0
942.19	0.009	0
944.38	0.011	0
946.56	0.009	0
948.75	0.004	0
950.94	-0.003	0
953.12	-0.011	0
955.31	-0.019	0
957.5	-0.025	0
959.69	-0.029	0.001
961.88	-0.031	0.002
964.06	-0.028	0.003
966.25	-0.021	0.004
968.44	-0.008	0.006
970.62	0.012	0.009
972.81	0.044	0.012
975	0.105	0.017
977.19	0.214	0.023
979.38	0.396	0.03
981.56	0.679	0.036
983.75	1.078	0.044
985.94	1.599	0.057
988.12	2.278	0.076
990.31	3.185	0.097
992.5	4.394	0.117
994.69	5.977	0.133
996.88	8.008	0.144
999.06	10.559	0.149
1001.25	13.688	0.155
1003.44	17.196	0.16
1005.62	20.675	0.166
1007.81	23.743	0.17
1010	26.075	0.172

ERA40

psl	const	slope
940	0	0
942.19	-0.006	0
944.38	-0.008	0.001
946.56	-0.007	0.001
948.75	-0.003	0
950.94	0.003	0
953.12	0.011	-0.001
955.31	0.02	-0.001
957.5	0.029	-0.002
959.69	0.036	-0.002
961.88	0.041	-0.002
964.06	0.042	-0.001
966.25	0.038	0
968.44	0.028	0.001
970.62	0.011	0.003
972.81	-0.005	0.005
975	0.002	0.008
977.19	0.051	0.01
979.38	0.135	0.013
981.56	0.243	0.018
983.75	0.395	0.023
985.94	0.627	0.03
988.12	0.966	0.038
990.31	1.426	0.046
992.5	2.036	0.056
994.69	2.868	0.064
996.88	3.997	0.068
999.06	5.489	0.069
1001.25	7.397	0.068
1003.44	9.594	0.066
1005.62	11.809	0.064
1007.81	13.787	0.062
1010	15.314	0.061

ECHAM5

psl	const	slope
940	0	0
942.19	0.01	0
944.38	0.014	0
946.56	0.012	0
948.75	0.005	0
950.94	-0.004	0
953.12	-0.016	0.001
955.31	-0.028	0.001
957.5	-0.038	0.001
959.69	-0.045	0.002
961.88	-0.047	0.002
964.06	-0.043	0.002
966.25	-0.032	0.001
968.44	-0.01	0
970.62	0.022	-0.001
972.81	0.063	-0.003
975	0.104	-0.003
977.19	0.146	-0.002
979.38	0.23	0
981.56	0.404	0.002
983.75	0.688	0.005
985.94	1.086	0.007
988.12	1.657	0.009
990.31	2.523	0.011
992.5	3.765	0.013
994.69	5.344	0.018
996.88	7.211	0.026
999.06	9.359	0.04
1001.25	11.788	0.062
1003.44	14.348	0.09
1005.62	16.771	0.12
1007.81	18.802	0.148
1010	20.219	0.171

HIRHAM

psl	const	slope
940	0	0
942.19	0.004	-0.002
944.38	0.006	-0.002
946.56	0.005	-0.002
948.75	0.002	-0.001
950.94	-0.002	0.001
953.12	-0.007	0.004
955.31	-0.013	0.007
957.5	-0.017	0.011
959.69	-0.02	0.014
961.88	-0.02	0.016
964.06	-0.017	0.017
966.25	-0.009	0.016
968.44	0.004	0.012
970.62	0.023	0.006
972.81	0.043	0.003
975	0.05	0.017
977.19	0.039	0.058
979.38	0.051	0.116
981.56	0.138	0.175
983.75	0.326	0.217
985.94	0.628	0.221
988.12	1.09	0.176
990.31	1.804	0.073
992.5	2.808	-0.074
994.69	4.004	-0.21
996.88	5.288	-0.28
999.06	6.667	-0.286
1001.25	8.183	-0.253
1003.44	9.732	-0.203
1005.62	11.088	-0.154
1007.81	12.042	-0.124
1010	12.417	-0.133

References

Benestad, R.E., 2002. Empirically downscaled multi-model ensemble temperature and precipitation scenarios for Norway. *Journal of Climate*, **15**, 3008–3027.

Benestad, R.E., 2004. Empirical-Statistical Downscaling in Climate Modeling. *Eos*, **Volume 85**(42), p. 417.

Benestad, R.E., 2005a. Climate change scenarios for northern Europe from multi-model IPCC AR4 climate simulations. *Geophys. Res. Lett.*, **32**(doi:10.1029/2005GL023401), L17704.

Benestad, R.E., 2005b. A review of the solar cycle length estimates. *Geophys. Res. Lett.*, **32**.

Benestad, R.E., & Chen, D., submitted. The use of a Calculus-based Cyclone Identification method for generating storm statistics. *Tellus*.

Benestad, R.E., & Hanssen-Bauer, I., 2003. *Empirical-based refinement of dynamically downscaled temperature scenarios in southern Norway*. KLIMA 07/03. The Norwegian Meteorological Institute, PO Box 43 Blindern, 0313 Oslo, Norway (www.met.no).

Blackmon, M. B., Boville, B., Bryan, F., Dickinson, R., Gent, P., Kiehl, J., Moritz, R., Randall, D., Shukla, J., Solomon, S., Bonan, G., Doney, S., Fung, I., Hack, J., Hunke, E., Hurrell, J., & et al., 2001. The Community Climate System Model. *Bull. Amer. Meteor. Soc.*, **82**, 2357–2376.

Christensen, J.H., Christensen, O.B., Lopez, P., van Meijgaard, E., & Botzet, M., 1996. *The HIRHAM4 Regional Atmospheric Climate Model*. DMI Sci. Rep. No. 96-4. Danish Meteorological Institute, Lyngbyvei 100, DK-2100 Copenhagen.

Delworth, T.L., Broccoli, A.J., Dixon, K., Held, I., Knutson, T.R., Kushner, P.J., Spelman, M.J., Stouffer, R.J., Vinnikov, K.Y., & Wetherald, R.E., 1999. Coupled Climate Modelling at GFDL: Recent Accomplishment and Future Plans. *Pages 15–20 of: CLIVAR Exchanges*, vol. 4. CLIVAR.

Geng, Q., & Sugi, M., 2001. Variability of the North Atlantic Cyclone Activity in Winter Analyzed from NCEP-NCAR Reanalysis data. *Journal of Climate*, **14**, 3863–3873.

Giorgetta, M.A., Manzini, E., & Roeckner, E., 2002. Forcing of the quasi-biennial oscillation from a broad spectrum of atmospheric waves. *Geophys. Res. Lett.*, **29**(10.1029/2002GL014756).

Gordon, C., Cooper, C., Senior, C.A., Banks, H., Gregory, J.M, Johns, T.C., Mitchell, J.F.B., & Wood, R.A., 2000. The Simulation of SST, Sea Ice Extents and Ocean Heat Transports in aversion of the Hadley Centre Coupled Model without Flux Adjustments. *Climate Dynamics*, **16**, 147–168.

Hartmann, D.L., 1994. *Global Physical Climatology*. San Diego, USA: Academic Press.

IPCC., 2002 (11–13 June). *Changes in Extreme Weather and Climate Events*. http://www.ipcc.ch/pub/support/. Beijing, China.

Knippertz, P., Ulbrich, U., & Speth, P., 2000. Changing cyclones and surface wind speeds over the North Atlantic and Europe in a transient GHG experiment. *Climate Research*, **in press**.

Økland, B., & Berryman, A., 2004. Resource dynamic plays a key role in regional fluctuations of the spruce bark beetles Ips typographus. *Agricultural and Forest Entomology*, **6**(141-146).

Økland, B., & Bjørnstad, O.N., 2003. Synchrony and geographical variation of the spruce bark beetle (Ips typographus) during a non-epidemic period. *Population Ecology*, **45**, 213–219.

Økland, B., & Bjørnstad, O.N., in press. A resource depletion model of forest insect outbreaks. *Ecology*.

Peixoto, J.P., & Oort, A.H., 1992. *Physics of Climate*. AIP.

Simmons, A.J., & Gibson, J.K., 2000. *The ERA-40 Project Plan*. ERA-40 Project Report Series 1. ECMWF, www.ecmwf.int.

Skog & Forskning., 1995. *Vindar og vindskador [wind and wind damages]*. Tech. rept. 3/95. Skog & Forskning.

Smits, A., A.M.G. Klein Tank, & Können, G.P., 2005. Trends in storminess over the Netherlands, 1962–2002. *International Journal of Climatology*, **25**, 1331–1344.

Trenberth, K.E., & Stepaniak, D.P., 2004. The flow of energy through the earth's climate system. *Quarterly Journal of the Royal Met. Society*, **130**(603; doi 10.1256/qj.04.83), 2677–2701.

Ulbrich, U., & Christoph, M., 1999. A shift in the NAO and increased storm track activity over Europe due to anthropogenic greenhouse gas forcing. *Climate Dynamics*, 551–559.